Chapter 2
Technical Approach

Details regarding the technical approach employed in this study are discussed in the following subsections. The test rig, including plenums and test section, is considered first, followed by a discussion of the three measurement techniques, including their hardware and software configurations and operating principles.

2.1 Test Facility and Facility Design Objectives

In this section, the rig plenum chambers, test section design, pressure measurement devices, rig air supply system, and Mie scattering smoke generator are discussed.

2.1.1 Original, Modified, and Redesigned Plenum Chambers

The original facility selected for this study, designed and constructed by Dr. Ludwig Haber, has both inlet and outlet plenum chambers, as shown in Figure 2-1. Much greater detail regarding the original test facility can be found in his dissertation [5]. The inlet plenum contains three screens to reduce the inlet flow turbulence. The facility is configured for low pressure, non-reacting (cold) flow experiments, and can accommodate any cross section up to a width of 10.25 inches, a height of 10.5 inches, and a length of 48 inches.

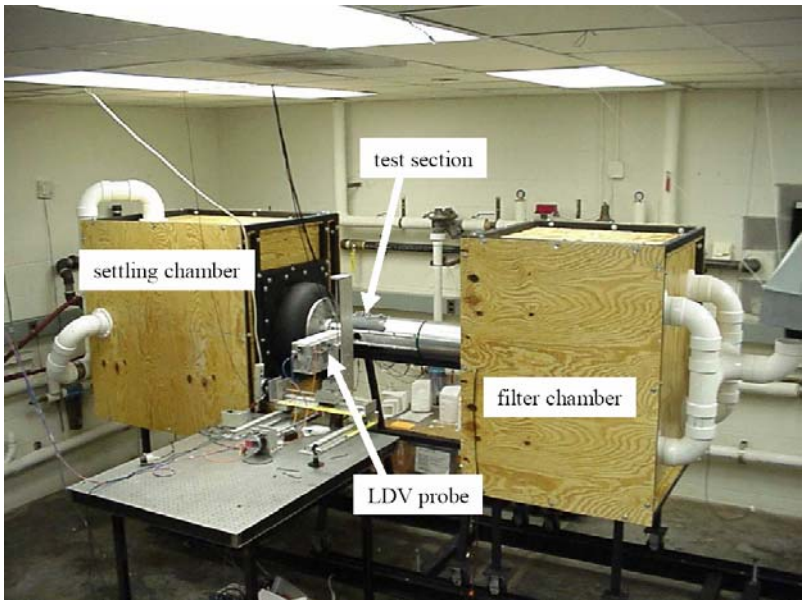

Figure 2-1. Original test facility designed and constructed by Dr. Haber. Image from [5].

The inlet plenum existing after the work of Haber has a steel frame with ½ inch thick plywood walls. The inner dimensions are 44 in x 36 in x 44 in. All wooden panels are bolted to the frame and joints are filled with silicon caulk. The outlet plenum has similar construction with inner dimensions of 33 in x 36 in x 44 in. The outlet plenum contains a heavy duty residential Hepa air filter to remove ceed particles before the flow is collected by four 4 inch diameter PVC pipes and directed into an exhaust duct.

These plenums were utilized at the beginning of the work, but were found to be unsuitable for the purposes of this study. The existing rig had been run with a variable swirl vane swirler and low pressure drop test section installed. With the swirler and test section generating less then 0.5 psi of back pressure on the plenum, leaks were not detected; however, operating at higher pressures caused major leakage and structural problems for the original plenum. Considerable energy and time was committed to modifying the original inlet plenum, repairing leaks and reinforcing the walls, only to achieve a 25% reduction in leakage flow. The attempted repairs followed an iterative process described in the following paragraph.

With the nozzle outlet sealed, the plenum was pressurized allowing any leaks to be discovered and marked. Plenum pressure was then relieved, and the marked leaks were sealed with silicon calk. The silicon required 24 hours to dry, after which time the

process of pressurization, detection, and sealing was repeated. Plenum pressure was incrementally increased between each iteration causing new leaks to form. Early efforts to seal the plenum involved sealing external leaks, but failed to produce significant results. Later efforts focused on sealing the plenum chamber from the inside as well as creating a reusable seal for the front panel, which must be removable for plenum access. Internal sealing had a greater effect on leakage flow than external sealing, but was still unable to substantially reduce the leakage. Many large joints and the porous wood made sealing the inlet plenum extremely difficult.

Joint expansion was another factor responsible for causing leakage. When pressurized, the front and rear panels of the inlet plenum began to bow out in the center, as illustrated in Figure 2-2, and along the edges between bolts. The bowing problem was significantly reduced by adding sections of steel 'U' and 'L' beams along the length of the plenum. These beams, shown in Figure 2-3, successfully prevented the joints around the front and rear panels from expanding and leaking under pressure. They also added strength to reduce the bowing at the center of each panel.

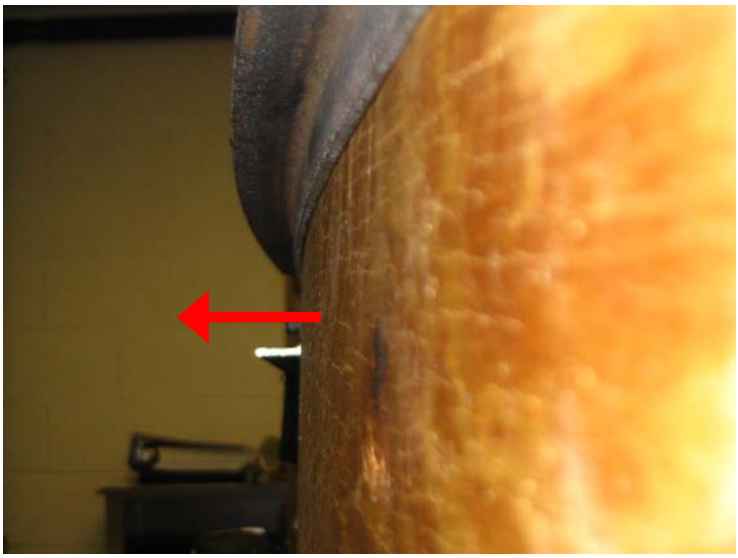

Figure 2-2. Profile view of inlet plenum rear panel under pressure, note outward bowing.

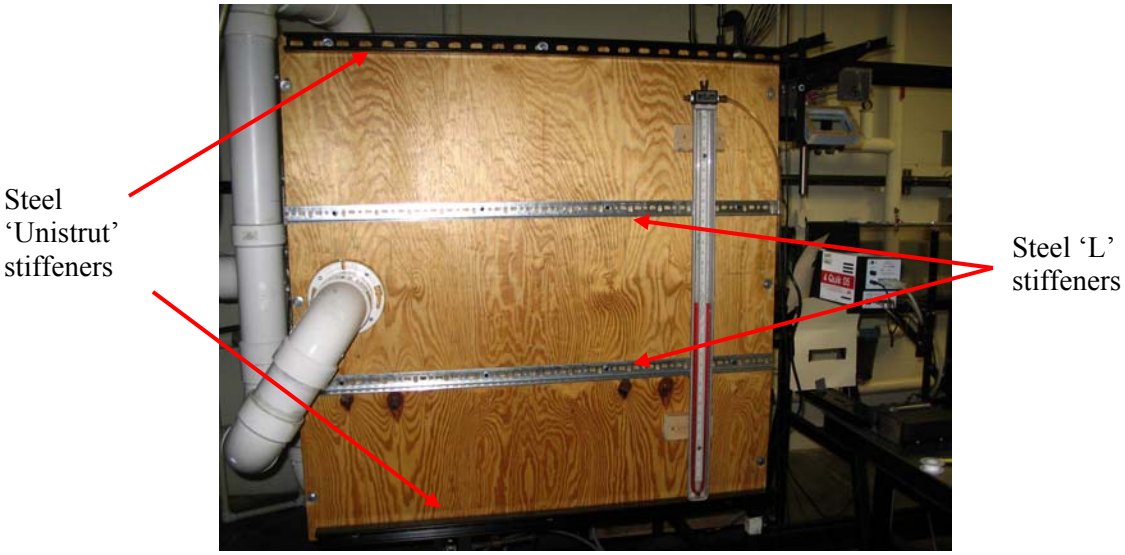

Figure 2-3. Inlet plenum front panel showing added steel beam stiffeners.

After the addition of the structural steel stiffeners, the plenum leaks persisted in other parts of the plenum. Even with the added stiffeners, there is still a risk of explosion if this inlet plenum is pressurized to several psi. With a mere 2 psi applied across the 1936 square inch front panel, the panel is holding a 3872 lb force. The panel bolts and plenum steel frame can easily handle that load, but the plywood is heavily stressed. The front and rear panels would be the first to fail. A burst of the plywood panel would certainly throw splinters, which could injure persons or damage equipment nearby.

After two weeks of sealing and reinforcement effort, the plenum leakage flow was measured by covering the nozzle outlet, pressurizing the plenum, and measuring the mass flow required to maintain pressure. For this measurement, plenum pressure was held at 0.9 psi, the pressure indicated by simulations needed to drive the on-design flow through Nozzle D. The leakage flow found was 95% of the desired mass flow through the nozzle. This amount of leakage was unacceptable because the RFL air supply system can only supply the sum of the nozzle and leakage air flows for a fraction of a minute, not long enough to run the desired experiments.

Because of the limited Reacting Flow Lab (RFL) air supply and persistent plenum leakage, another air supply became necessary. The RFL has a second source of compressed air from the Aerospace Engineering Department air compressor, which is capable of supplying both the nozzle and leakage air flows together. The total air flow

into the rig is measured, and if the leakage flow were known, the nozzle flow could be determined. The two nozzles tested require different back pressures, therefore the leakage flow must be known as a function of pressure.

To determine this relationship, measurements were made to characterize the leakage flow. By again covering the nozzle outlet, the leakage flow was measured at increasing 2-in H_2O increments in plenum pressure, and the plenum pressure vs. flow characteristic curve was plotted. Using this curve, shown in Figure 2-4, and its fit equation, the leakage mass flow can be found through measurement of the plenum pressure. The leakage flow is then subtracted from the total flow rate measured to determine the nozzle flow rate.

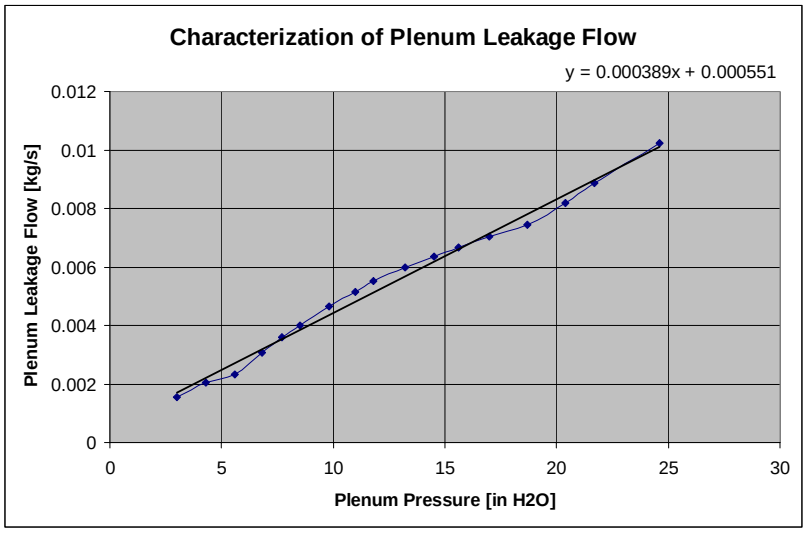

Figure 2-4. This image illustrates the results of the first plenum leakage flow characterization. Both the raw data (connected dots) and linear curve fit are shown.

The leakage flow characterization discussed previously was ultimately found to be less helpful than expected. The characterization was conducted five times over a few days with different results for each. These tests revealed a greater than 27% inconsistency between leakage flow measurements. Therefore, the conclusion was drawn that a simple characterization of the plenum leakage flow would not be sufficient enough to accurately determine the desired nozzle flow rate. For that reason, the original plenum was deemed unusable for the desired measurements, and a new inlet plenum was needed.

A new inlet plenum was designed to mount inside the original plenum with two main goals. First, the new plenum needed to be leak-free at the required backpressure and secondly, it was necessary to provide the test section with low turbulence air and a uniform flow profile. The criterion for a low turbulence uniform inlet flow allowed the plenum extension inlet condition to match the inlet condition employed in the CFD simulations. The new plenum, shown in Figure 2-5, is constructed from an 8 inch diameter, 32 inch long, schedule 40 PVC pipe. The inlet end is capped with a glue-on end cap and air enters radially through four ½ inch SWAGELOK tube connections. Air enters the plenum into an open section of pipe, then passes through a 4 inch thick layer of packed Polyester quilt batting for turbulence reduction, and finally through a ½ inch thick honeycomb layer to generate more uniform flow. The outlet end of the new plenum connects to the inlet plenum extension through a hole in the original plenum wall. The new plenum is bolted to the wall opening via a 12 bolt Plexiglas flange glued onto the pipe. Like the flange, the wall is made of Plexiglas, so a thin layer of silicon caulk provides a leak proof seal between the wall and flange.

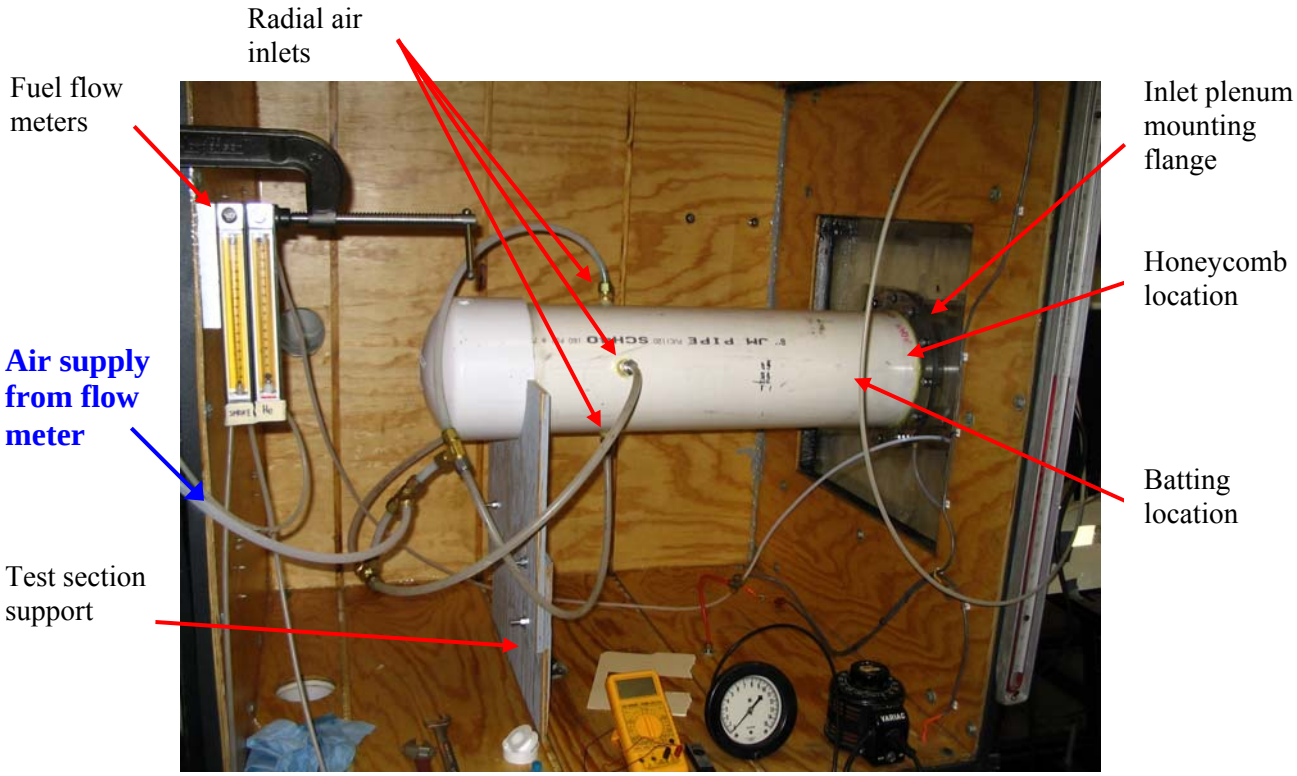

Figure 2-5. New inlet plenum with major components indicated. For the 'fuel' flow, oil smoke is used in the Mie scattering experiments and helium in the schlieren experiments.

The fuel flow meters shown in Figure 2-5 are each Matheson rotameters. A model 603, on the left, is used to meter the smoke flow and a model 604, on the right, is used to meter helium flow. Each of these flow meters is calibrated using the intended gas against a dry gas flow meter from Singer. The calibration data is used to convert the rotameter reading into a flow rate in kg/s.

2.1.2 Test Section Considerations

The test section employed in this study has two major components, the inlet plenum extension and the test section itself. The actual test section is described first. As discussed in the previous paragraphs, the test section design drove the new inlet plenum design. The test section was initially designed to simulate the geometry of an engine burner and also provide optical access necessary for LDV, Mie scattering flow visualization and schlieren measurements. The PT6 engine, for which Nozzles D and J are designed, has an annular burner can, which is simulated by straightening a 25% sector of the annulus into a rectangular test section 2.5 inches wide by 9.375 inches tall. This concept is illustrated in Figure 2-6.

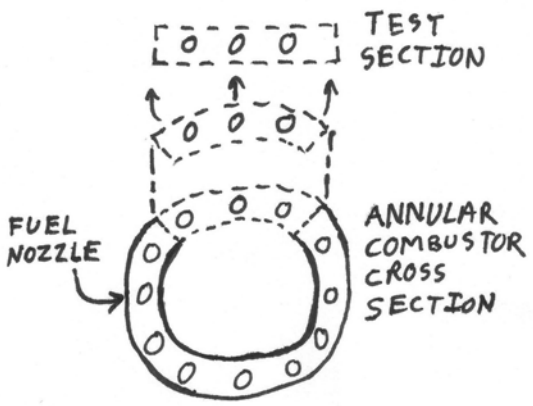

Figure 2-6. Illustration of the concept described in the previous paragraph to select a test section geometry.

Swappable inlet end plates were constructed to allow either one or three nozzles to be tested. The ability to mount three nozzles provides the opportunity to study the

fluid interaction between nozzles. The test section is 36 inches long, which allows it to fit between the two plenums, and be supported by the existing structure. Figures 2-7 and 2-8 illustrate both ends of the test section.

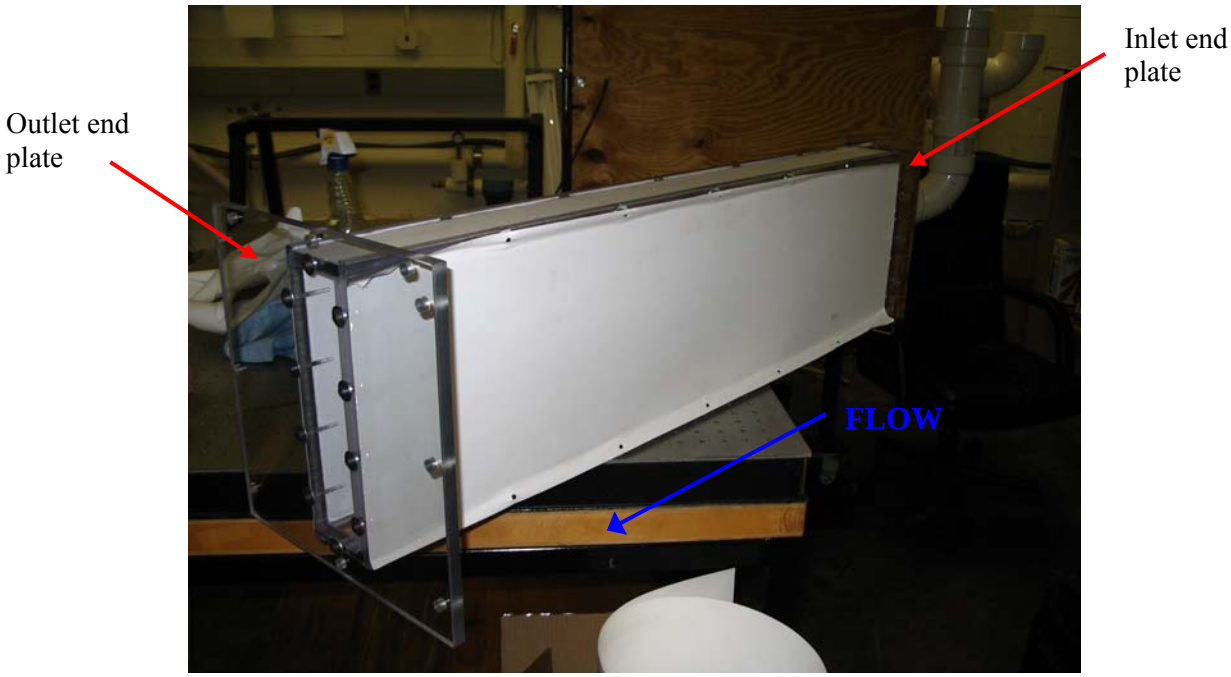

Figure 2-7. Test section, upstream view showing protective coating on sides and top.

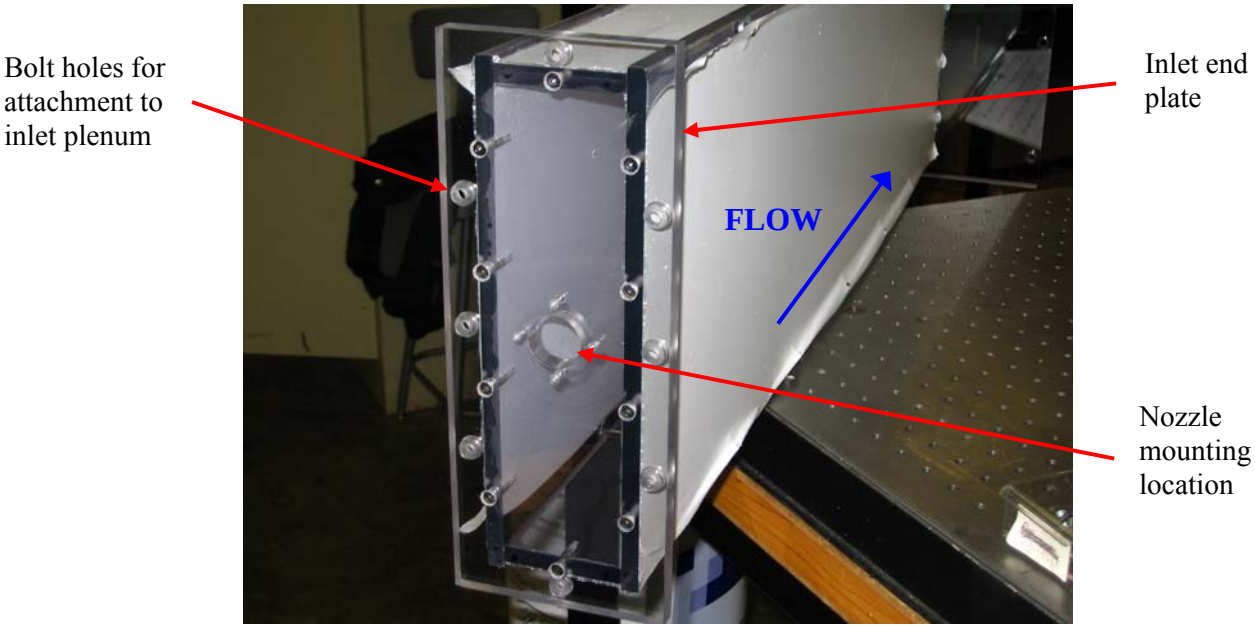

Figure 2-8. Test section, downstream view with single nozzle inlet end plate installed.

The flat walls allow direct optical access and greatly reduce the complexity of the post processing required for the experimental results. All joints in the test section were designed for screw connection, and care was taken to locate screws so as to avoid blocking the optical path to the nozzle outlet flow in both single and multiple nozzle cases. A small bead of clear silicon calk was applied between panels to prevent leakage. Screw fastening was selected for the section so that it could be readily disassembled if necessary for cleaning or modification. If disassembly is required in the future, care should be taken to remove all traces of old silicon, and a tap should be run any threads to clean them before reassembly. Care must be taken when tightening screws into threaded Plexiglas because over-tightening can easily lead to cracking.

An inlet plenum extension is required to locate the test section out and away from the large plenum chamber allowing physical access for the LDV probe to make measurements immediately downstream of the nozzle. The inside height and width of the extension are the same as the test section, but it is only 6 3/4 inches long. Each of the Plexiglas panels is glued together with "Weld-On" #16 Clear Acrylic Cement, and there is a flange on each end with a rectangular eight bolt pattern to permit attachment to the inlet plenum and test section. Because of the way the flange holes are, drilled or tapped, the extension can only be installed with the flow in one direction, which is indicated on the extension. The extension can, however, be rotated 180 degrees about the rig z-axis and installed properly. Figure 2-9 shows a picture of the plenum extension.

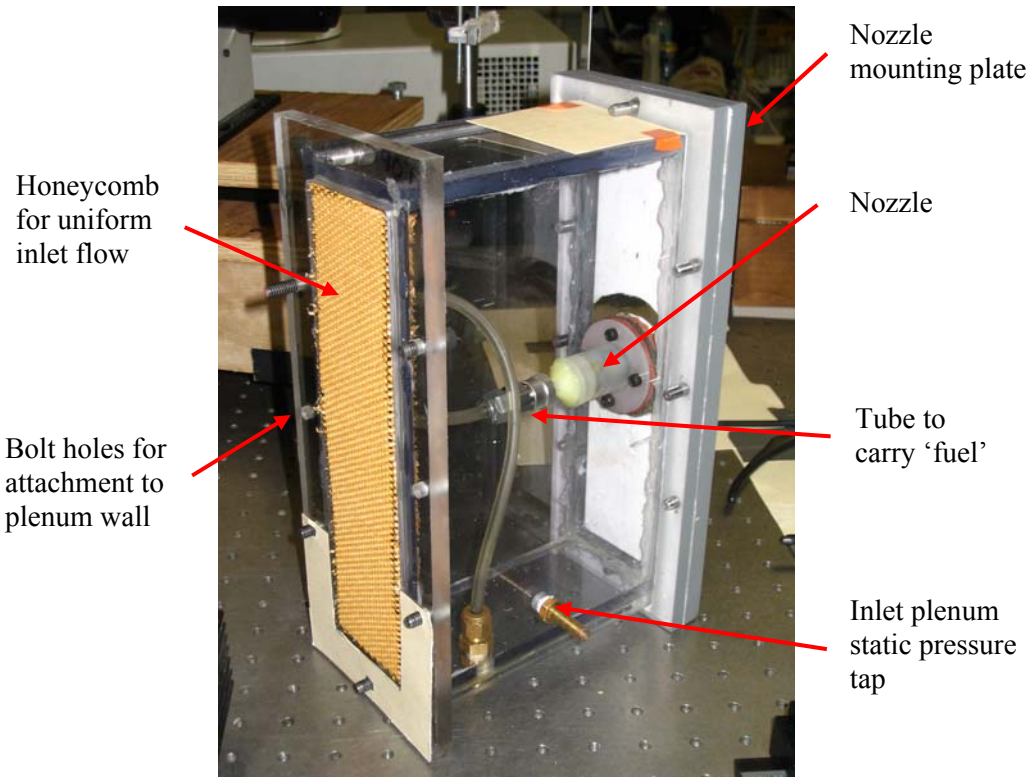

Figure 2-9. Picture showing the inlet plenum extension with nozzle mounting plate attached.

The extension bolts onto a 2 by 2 foot Plexiglas plate, which completes the plenum wall by bolting onto the original inlet plenum chamber. This large plate is required to fill the space previously occupied by the variable swirl vane swirler during past studies [5]. For installation, the subject nozzle is mounted in the test section, and the test section is bolted to the inlet plenum extension. The downstream end of the test section is bolted to the outlet plenum chamber.

During preliminary runs of both the Mie scattering flow visualization and schlieren systems, it was determined that Plexiglas was a poor material selection because of its optical properties. Either flat glass windows would need to be added to the test section or the experiments could be run without the test section, allowing the nozzle to exhaust into the ambient room environment. This proved to be the simplest and most economical option, and was pursued. New CFD models with modified boundary conditions were run to simulate the new geometry, dumping into an open ambient environment. The test section was completely removed, and the outlet plenum chamber was bypassed. The test section inlet plate, where a nozzle can be mounted, was removed

from the test section and bolted directly to the inlet plenum extension. The exhaust duct was extended down in place of the test section to draw away any helium or seed particles expelled from the nozzle. The final set up is shown in Figure 2-10.

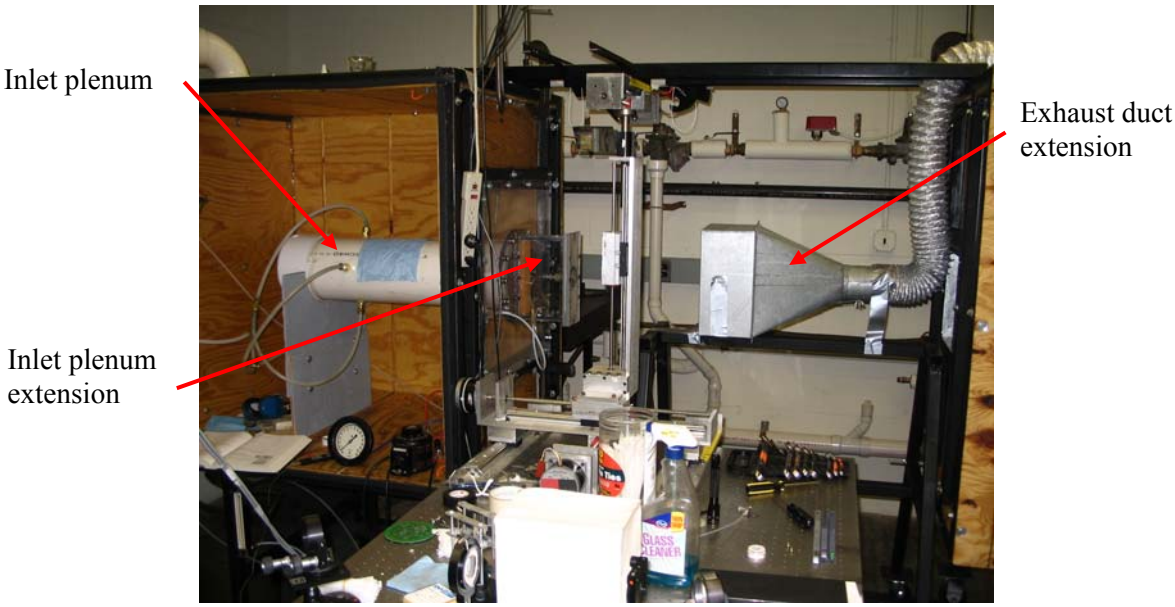

Figure 2-10. This figure shows the final configuration of the test rig. The test section is removed and the exhaust duct is extended to bypass the outlet plenum.

Silicon caulk was used effectively to seal test section joints and prevent leaks, but is difficult to remove and reapply if the joint is disassembled. For this reason, a gasket was used to seal the joint between the test section inlet plate and the inlet plenum extension. This joint must be disassembled and reassembled frequently to clean and change nozzles. The worn gasket can be used to cut a new gasket and should be replaced every two or three assemblies because the gasket material compresses over time and stops producing a reliable seal.

2.1.3 Gauge Pressure Measurements

The inlet plenum allows a back pressure to build behind the nozzle, which is then dumped to the ambient room air on the outlet side of the nozzle. This configuration allows the static pressure drop across the nozzle to be measured directly by measuring the

inlet plenum gage pressure. Initially, a water u-tube manometer with 36 inch differential pressure capability was installed on the rig to measure the inlet plenum pressure, as shown in Figure 2-11. A static pressure tap was installed just upstream of the nozzle on the side of the inlet plenum, as shown in Figure 2-9, to facilitate the measurement. The manometer was selected because its range gave it the ability to measure the 24 in H_2O pressure drop predicted by the CFD simulations for Nozzle D. After preliminary testing, it became clear that the nozzle pressure drop at the desired flow rate was higher than predicted, thus a pressure measurement device with a larger range was required. The manometer was a first choice for pressure measurement because it is simple to read and requires no calibration.

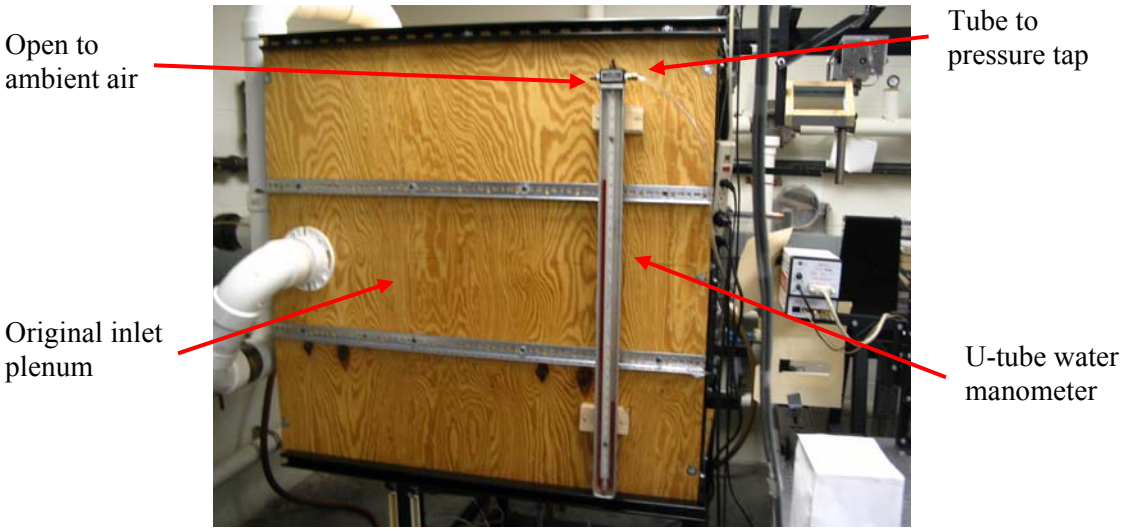

Figure 2-11. Manometer initially implemented to measure inlet plenum gauge pressure.

A Bourdon tube pressure gauge, shown in Figure 2-12, with a maximum range of 0-15 psi was selected to replace the manometer. This gauge was calibrated using a dead weight pressure tester across its entire range. The selected gauge contains an adjustable indicator used to zero the gauge. With the calibration curve, the gauge was successfully used for measurement of the static pressure drop across each nozzle. These pressure drops are reported and discussed later in Chapter 3.

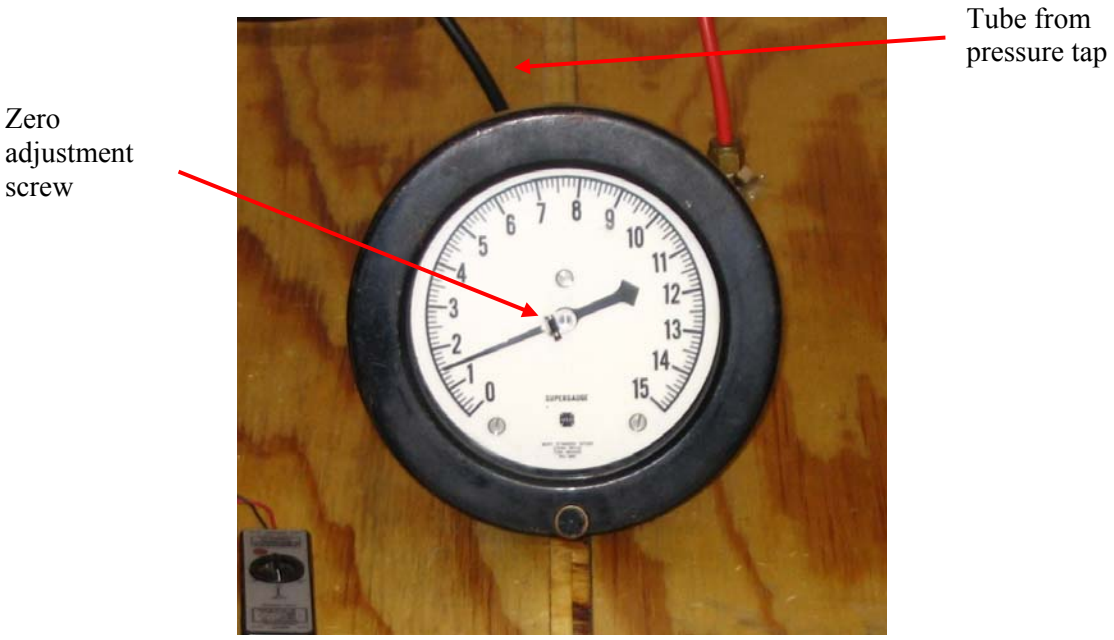

Figure 2-12. Bourdon tube pressure gauge selected to measure the inlet plenum gauge pressure.

2.1.4 Air Supply System

The original air supply system to the test facility has been modified with the capability to utilize compressed air from two separate sources, a Kaeser compressor in the RFL and a high pressure compressor in the Aerospace Engineering wing of Randolph Hall. The air supply system allows the user to switch between air sources and regulate the supply pressure from 0 to 125 psi. The abilities to control and measure the mass flow rate are also included in the air supply system. Appendix E is included as a reference and contains greater details regarding the design and function of the air supply system. Appendix D includes information about the air compressor owned by the Aerospace Engineering Department along with a manual for its operation.

2.1.5 Smoke Generator

A continuous source of uniform smoke is required to properly 'contaminate' the nozzle flow and scatter light for the Mie scattering flow visualization experiments. An existing smoke generator, originally designed by Steve LePera of Virginia Tech, is

implemented in this study and two major improvements are made. The smoke generator, shown in Figure 2-13, has two chambers. The first contains a coil of resistive heater wire on the surface of an oil bath to generate smoke, and the second contains tightly packed cotton, which acts as a filter chamber to remove large oil droplets and allow the smoke and clean air to mix uniformly before traveling to the test section. SAE 30-weight motor oil is vaporized in this generator. The heater wire coils in and out of the oil bath at the oil/air interface, where smoke is generated. The smoke mixes with clean air from the ½ inch o.d. air inlet and travels through a ½ inch o.d. copper tube to the filter chamber. The copper tube was installed after the original plastic tube melted from the heat of the smoke.

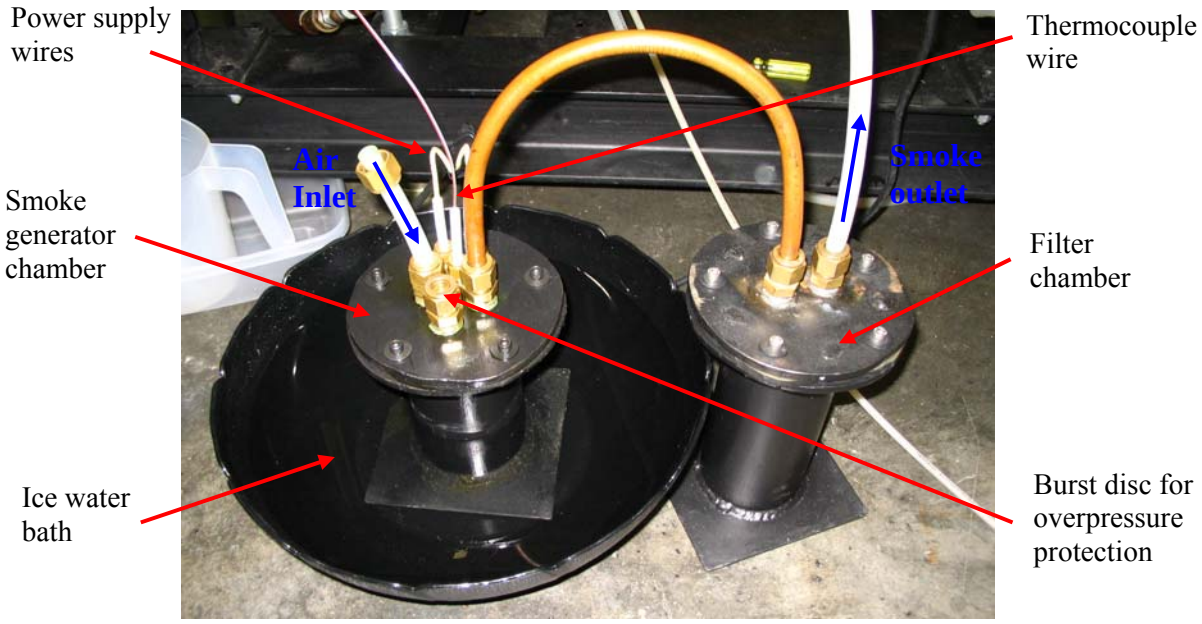

Figure 2-13. Smoke generator used in Mie scattering flow visualization experiments. In this image, the smoke generation chamber is placed in an ice water bath for cooling.

As the heater temperature is increased, thicker and darker smoke is generated. Ideally, for safety, the oil should only be heated and vaporized as it comes in contact with the heater wire, but the entire oil bath is heated in this implementation. The bath is heated to a temperature between the smoke and flash point temperatures of the oil; therefore if the temperature is not monitored closely a fire could ignite. A fire did occur during initial testing, which melted the electrical insulation within the generator. The generator was repaired and a thermocouple was installed to monitor the oil bath

temperature. Type J thermocouple is connected to an electric cold reference compensator and the output is read on a multimeter. The multimeter reading should be kept below 13.5 mV (~460°F) to prevent fire. With an ice water bath for cooling, the supply voltage could be raised as high as 45 Volts with continuous operation. Figure 2-14 illustrates the smoke generator and auxiliary equipment along with a sketch of the thermocouple location.

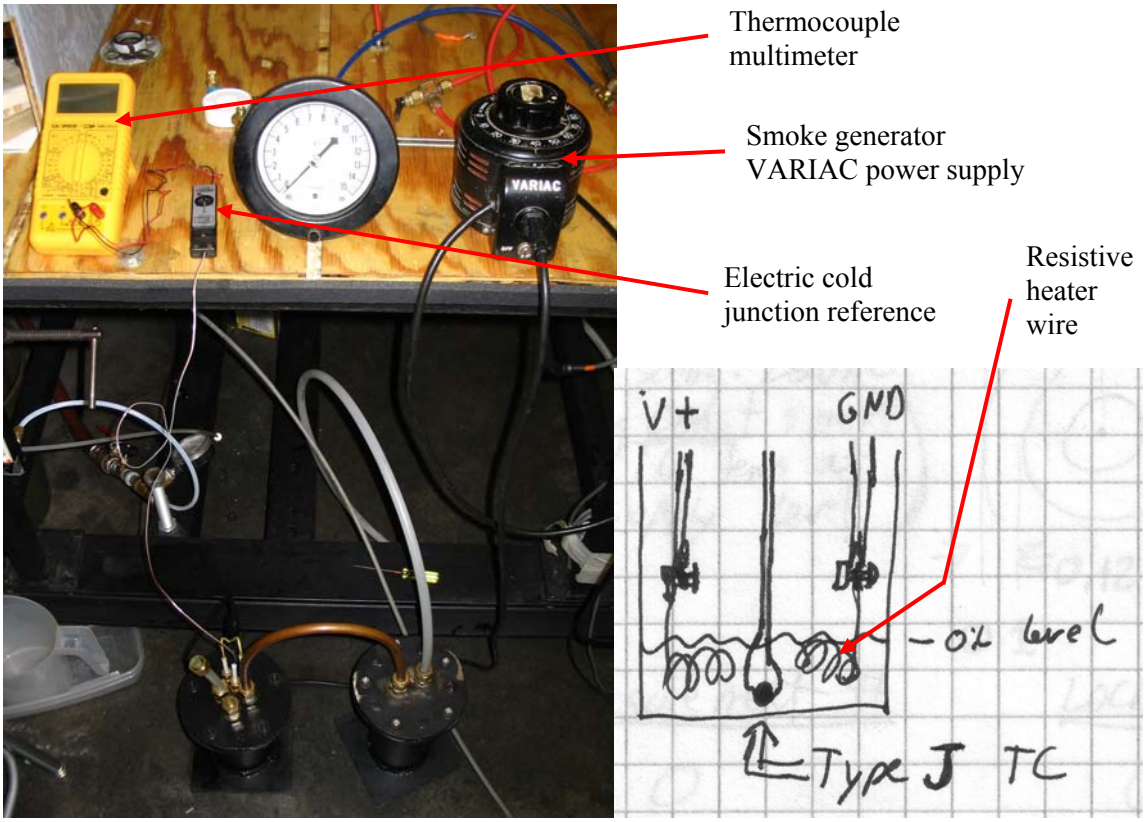

Figure 2-14. Image of smoke generator showing auxiliary equipment and sketch of thermocouple location.

2.2 The Employed Measurement Techniques

In this study, four main comparisons are drawn between the experimental and computational results: relative fuel concentration uniformity and spatial distribution, overall swirl angle, general geometric features of the flow, and velocity profile. To measure these characteristics, three measurement techniques are employed: Mie

scattering laser sheet flow visualization, schlieren flow visualization, and Laser Doppler Velocimetry (LDV). The following sub sections explain, in detail, the operating principles and theory behind each technique along with its physical implementation and desired results.

2.2.1 Mie Scattering Flow Visualization System

In this study, the Mie scattering flow visualization experiment is used to qualitatively evaluate several properties of the nozzle outlet flow. Flow properties evaluated include: relative fuel concentration uniformity and spatial distribution, overall swirl angle, and general geometric features of the flow. For this measurement technique, a thin sheet of laser light is passed through a flow seeded with particles. These particles scatter laser light, which can be detected with a camera. The seed particles used are small and carry very little inertia, so they can be assumed to properly follow the flow. Oil smoke is used as seed in this study. Smoke is injected through the nozzle 'fuel' inlets, and mixes with the air passing through the nozzle. In this way, the concentrations of smoke in the experimental results should match the concentrations of fuel in the CFD results.

The laser sheet is produced from a beam through an optical train incorporating a laser light source and a series of mirrors and lenses to position, aim, and condition the beam before it passes through a pair of cylindrical lenses, which fan the beam out into a sheet. Once created, the sheet is guided by three mirrors into the test section. The first of these mirrors directs the sheet 90 degrees from a direction parallel to the optical table to vertical. The second mirror turns the sheet back to horizontal, but well above the test section. The third mirror, which steers the beam down to the test section, is mounted directly above the test section on a single axis translation stage. This stage is responsible for moving the sheet across the test section, essentially allowing any z-y plane to be cut and photographed. The direction of translation is along the x-axis of the experiment. Because of its alignment, a 1 inch translation of the mirror results in a 1 inch horizontal translation of the sheet as it travels across the test section.

The laser used is a Spectra-Physics model 2020 argon laser, which produces a broadband beam of 450 nm to 600 nm at approximately 0.50 W when measured just downstream of the laser. The first mirror after the laser picks off the entire beam on the LDV optical table and directs it across the room to the laser sheet optical table. Once there, a second mirror steers the beam into the laser sheet optical train containing mirrors and lenses. The first lens takes the divergent beam from the laser head and makes it converge. Then the second lens reduces the convergence so that the beam is collimated, meaning that it neither converge or diverges. The second lens is located at the focal point of the first lens to provide the smallest possible beam diameter. This small diameter, nearly collimated beam, is properly conditioned to enter the sheet forming optics. Following the second lens, a third mirror directs the conditioned beam into a pair of cylindrical lenses, which form the sheet. The first cylindrical lens controls the sheet thickness, while the second spreads the beam into a sheet of uniform thickness and the second cylindrical lens is slow (long focal length) so the sheet width fills the test section area of interest, but does not spread out any further. Unnecessary spreading leads to reduced laser intensity in the area of interest. An optical path length from the first cylindrical lens to the test section was established so that the sheet would be as thin as possible at the location of interest, thus allowing for accurate illumination of only the plane of interest. A wider sheet would provide an average image of several thin planes.

With the previously discussed set up, a 1.5 mm thick laser sheet was created. The translation stage can easily translate the sheet in increments as small as 0.5 mm. Therefore, the maximum resolution of the experiment is limited to 1.5 mm, the sheet thickness. Appendix A contains additional information regarding: the optical set up of this experiment, maintenance tasks, and an in-depth procedure for making measurements.

Mie scattering images are captured by a black and white high speed intensified camera. Images are passed from the camera continuously at a rate based on the exposure time set by the user. A video capture card in the image processing computer is used to capture the images into memory. LabVIEW Virtual Instruments (VIs) are used to control the video capture card and perform some image processing, while the majority of image post processing is performed by a program written in MATLAB. The settings of the

intensified camera are controlled through a serial Hyper Terminal connection via the image processing computer.

The intensified camera, used for image capture, is a model 4 Quik 05 manufactured by Stanford Computer Optics, Inc. A camera equipped with an intensifier was required for this experiment because of the low intensity of the light sheet. Initially, two other cameras were implemented without success because of the low subject intensity. A Cohu digital camera and Sony Camcorder were both tried as capture devices before the need for an intensified camera was realized. The high amount of air mixing with the smoke flow in the nozzle diluted the smoke causing the low intensity. Before switching to the intensified camera, the smoke generator and laser settings were improved to optimize the intensity of scattered light. But even after optimization, the intensified camera was still found necessary.

Inside the camera, light passes through the focusing lenses and then through the charged intensifier plate, which acts as a light amplifier. The amplified light is then focused onto an optoelectric plate, which converts the image into an electric signal. Through the camera's serial connection, the exposure time and intensifier voltage can be adjusted. The camera gain is adjusted on the rear panel of the camera, as indicated in Figure 2-15. Increasing the camera gain directly brightens the image without loss of resolution. The image intensity can be increased by increasing the intensifier voltage; however, an excessive voltage setting will add noise to the image and it will become grainy and appear unfocused. The image intensity can be further increased by lengthening the exposure time. This increase is also limited because the exposure time cannot be longer than the time scale of the dynamics which are to be captured.

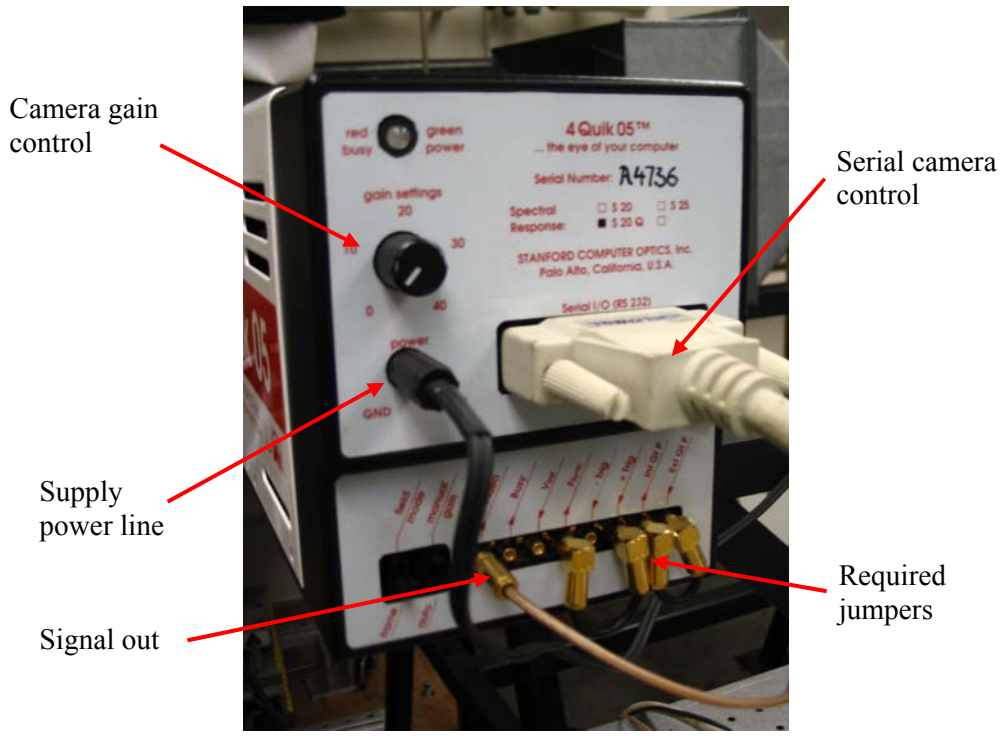

Figure 2-15. Rear panel of intensified camera showing location of camera gain control.

Five camera lens combinations with different focal lengths and aperture sizes were available for use. Each lens combination was tested to find its optimal setting, and these settings were recorded along with a description of the results for comparison. This process led to the selection of an optimal lens combination and camera location. The Tamron SP 90mm was selected with an aperture setting of 1:2.5. Using the Tamron lens, the best camera to subject distance was found to be 22 inches, measured from the nozzle center to the most forward point on the camera housing. The line of sight of the camera is perpendicular to the plane of interest, which required it to be located on the laser sheet optical table, where it is mounted on an adjustable support. The support, shown in Figure 2-16, allows the y and z locations of the camera to be adjusted in increments of a 1/2 inch. The x location can be adjusted in 1 inch increments. The camera support also allows at least ten degrees of rotation about each axis. These adjustment features permit optimization of the camera position.

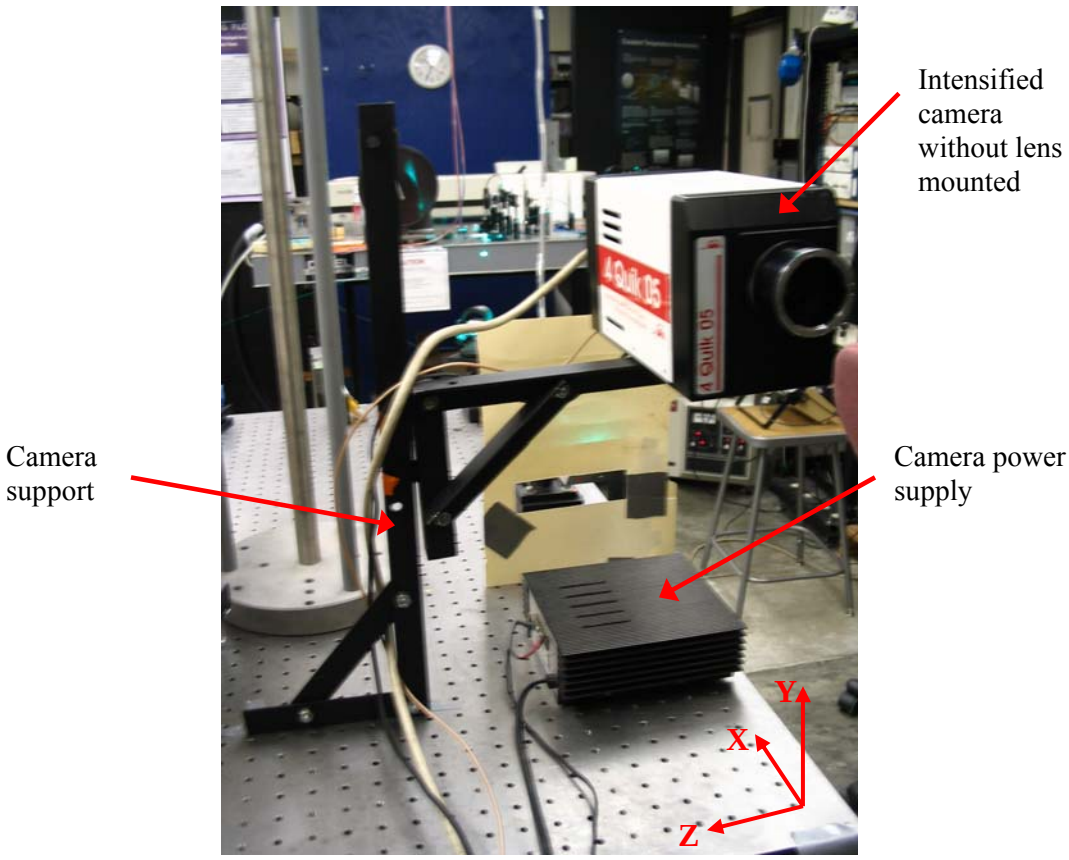

Figure 2-16. Intensified camera support bracket with built in adjustment features.

Two VIs were created to record images from the camera: 'CapturewithAverage.vi' and 'VideoCapture.vi.' Front panels both of VIs are shown in Figure 2-17. The video capture VI can record a (*.avi) video file by capturing a sequence of still frames and assembling them into a video. The user controls the total number of seconds of video to record, the frame rate, and the location and name of the video created. The second VI captures a sequence of still frames from the camera, averages them together, and then saves the averaged image. The user controls the number of frames to be averaged and the location and name to save the averaged file. By default, this VI displays a live view of the stream of images from the camera. The VI will capture and save an average when instructed by the user by switching the 'Average?' toggle.

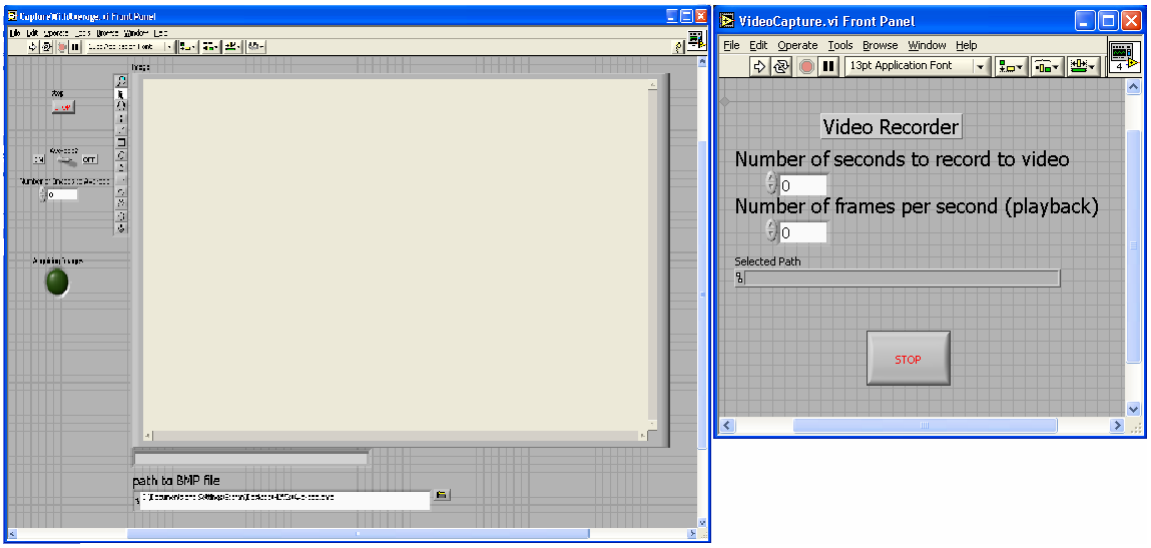

Figure 2-17. Front panel views of both 'CapturewithAverage.vi' and 'VideoCapture.vi.'

For each flow condition, two videos are recorded: one ten second video with the laser sheet positioned at the center line of the nozzle, and one fifteen second video showing the sheet being scanned across the flow along the x-axis. Video files are saved without any post processing, and are used to gain insight into the flow geometry and fuel/air mixing characteristics.

At each flow condition, fifteen averaged images are recorded. Averages are recorded at 1/16 inch intervals from negative 0.625 inches to positive 0.625 inches. The origin of the experiment is on the surface of the nozzle and in the nozzle center in both the x and y directions. At each location, fifteen images are captured and averaged, resulting in one saved averaged image per measurement location. Each of these average images is post processed by a MATLAB m-file written for that purpose. The program, 'contour.m' is run and calls four other programs to process the averaged image. 'Contour.m' first calls 'scale.m' to use information from a reference image to adjust the aspect ratio so that the x and y axis pixels per inch resolutions are equal. The difference in resolution is caused by the aspect ratio of the image capture device in the intensified camera. Contour then calls 'cut.m' to cut off the downstream part of the image because it is not necessary for comparison. 'Scale2.m' is then called, which uses the nozzle geometry in each image to scale the image size up to match the CFD image, while conserving aspect ratio. 'Contour_design.m' is then called. This program takes the

properly sized image and rescales the image intensity to utilize the full intensity range, 0 to 255. Intensities are rescaled by taking the minimum intensity and setting it to zero, taking the maximum intensity and setting it to 255, then rescaling the all other pixels correspondingly. Each pixel is then sorted into one of a user-controlled number of intensity bins. A new image is then created, which is colored based on which intensity bin each pixel falls into. The end result is a color contour plot of relative fuel concentration that is sized so it can be overlaid onto the CFD results. To show the effect of contouring, Figures 2-18 and 2-19 are provided, which show an averaged image before processing and after contouring respectively.

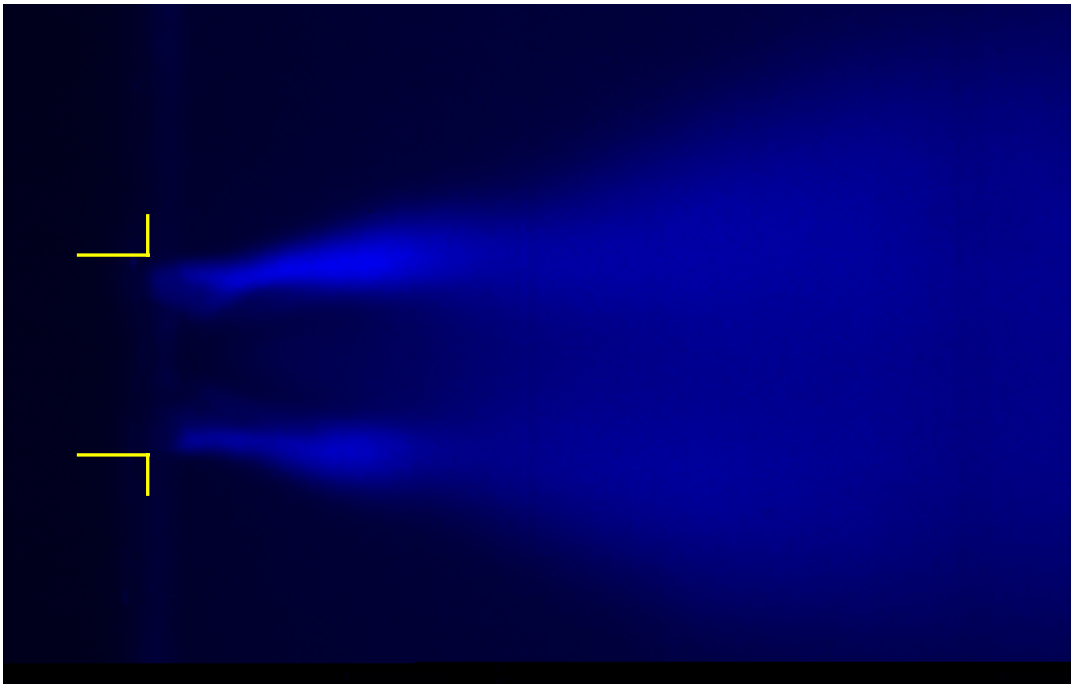

Figure 2-18. Averaged flow visualization image as recorded from the capture VI. The yellow lines indicate the outer boundaries of the nozzle outlet.

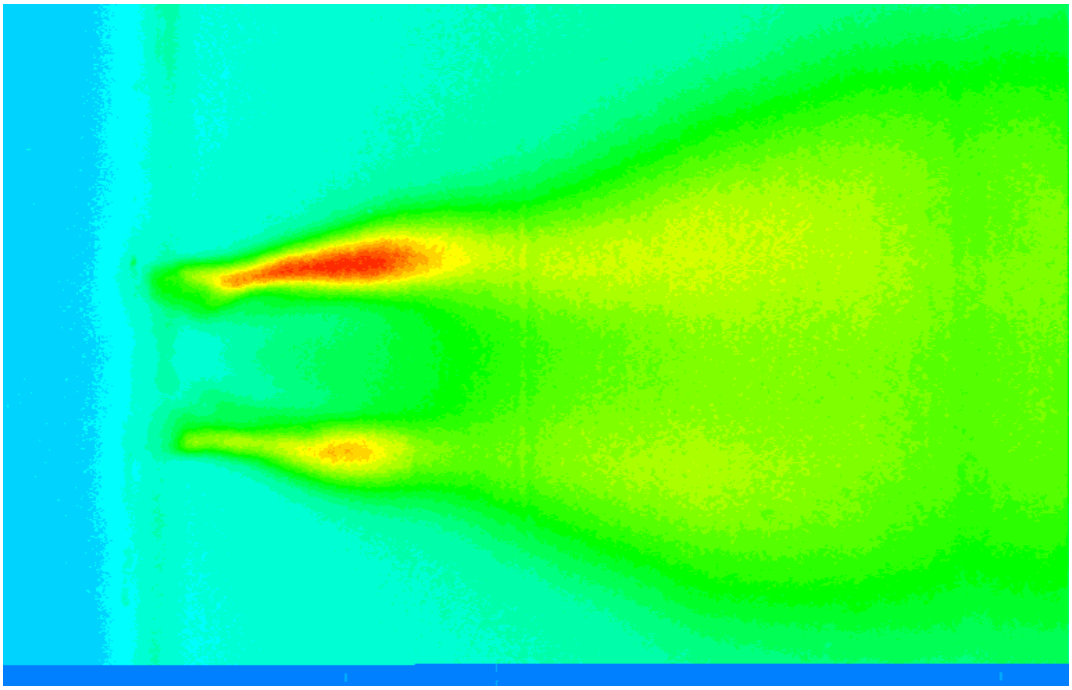

Figure 2-19. Averaged image shown in previous figure after being processed with 'contour_design.m.'

After contouring and resizing the averaged images, they are further processed with 'compare.m' to overlay the processed image on an image captured from CFD. The CFD results presented are for the same locations as the averaged images from the experiment. The CFD results show velocity vectors colored by fuel concentration. These concentrations have been scaled so that the maximum concentration in the image is scaled up to red and the minimum concentration is scaled down to blue. This sets the concentrations in both images on relative scales so they can be directly compared. The length of the velocity vectors gives an indication of the velocity magnitude. Figure 2-20 shows a fully processed and overlaid sample image. In the images presented in Chapter 3, the simulation image colors are inverted to provide increased clarity of the velocity vectors. The concentration contours in the flow visualization images are colored according to the scale shown in Figure 2-20 with red signifying a high concentration and blue signifying a low fuel concentration.

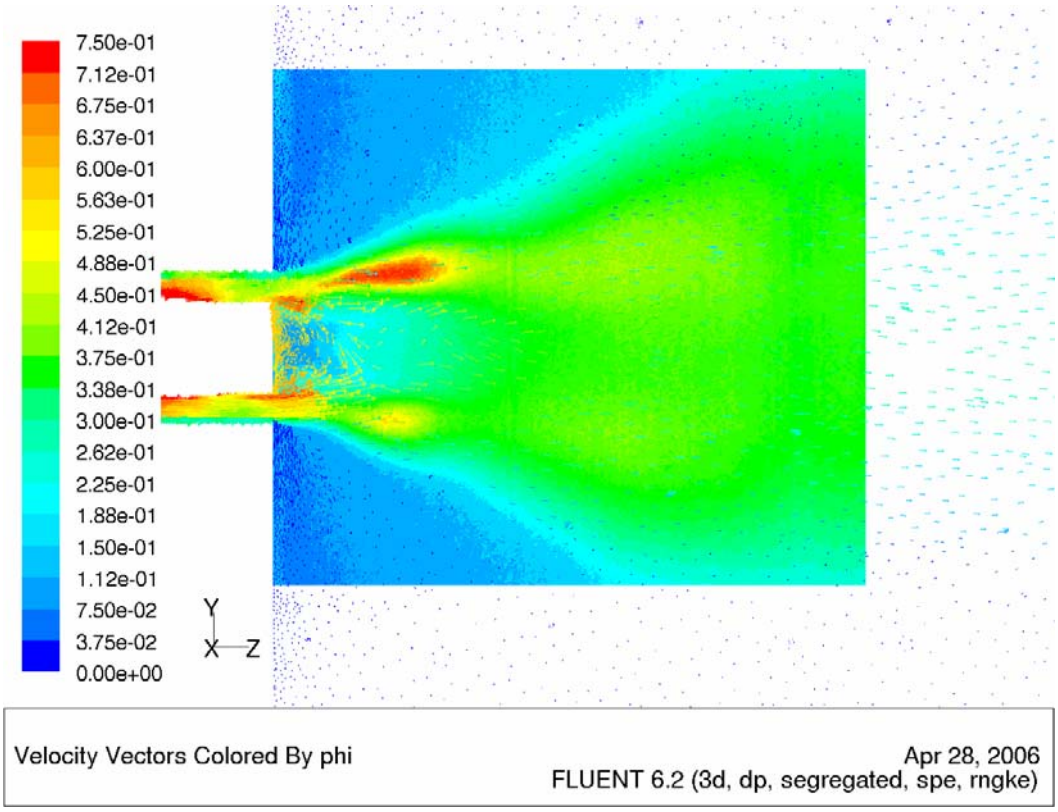

Figure 2-20. Fully processed image with flow visualization results overlaid on the CFD results.

2.2.2 Schlieren Flow Visualization System

As described earlier in section 1.2.2, schlieren flow visualization is a technique which detects variations in the index of refraction in a transparent medium through the resulting effects on a beam of collimated light passing through the test section [3]. Variations in the index of refraction are caused by density gradients in the fluid, which in the case of this study, are created by mixing fuel and air of different densities. A schlieren system incorporates a light source and lens which together establish a collimated beam of light passing through the test section. In the test section, across a boundary between two areas of differing density, there is a change in the index of refraction of the fluid. The light beam is turned in the direction of increasing index of refraction or toward the region of higher density [3]. After the test section, the beam passes through a second lens which focuses the collimated beam to a knife edge. The knife edge increases the contrast of the image, which is then captured by a digital camera.

Light from the source passes the knife edge and the deflected light is blocked, creating the light and dark areas seen in schlieren photographs.

The schlieren system indicates the first derivative of the index of refraction in a direction normal to the light beam [3]. Generally, the light is turned toward the region of higher density, in this case, the air. The schlieren results allow a qualitative investigation into the quality of fuel-air mixing inside and outside of the nozzle. As with the Mie scattering flow visualization, schlieren has the advantage of being a nonintrusive measurement technique. When used to make measurements of a three dimensional flow, such as the one under study, schlieren provides an average measurement of the flow along the collimated beam of light.

A traditional schlieren system set up as described above is shown in Figure 2-21. Large diameter, aberration-free lenses are required for this system, which greatly increases the cost. The large lenses are required to generate a collimated beam the size of the test section. In this implementation, nine inch diameter lenses would be required and are cost prohibitive. Fortunately, large parabolic mirrors can perform the same optically as lenses and are used in place of the lenses to reduce cost for this study. The schlieren system incorporating parabolic mirrors is illustrated in Figure 2-22. In this implementation, the angle α is kept as small as possible to reduce the effects of astigmatism.

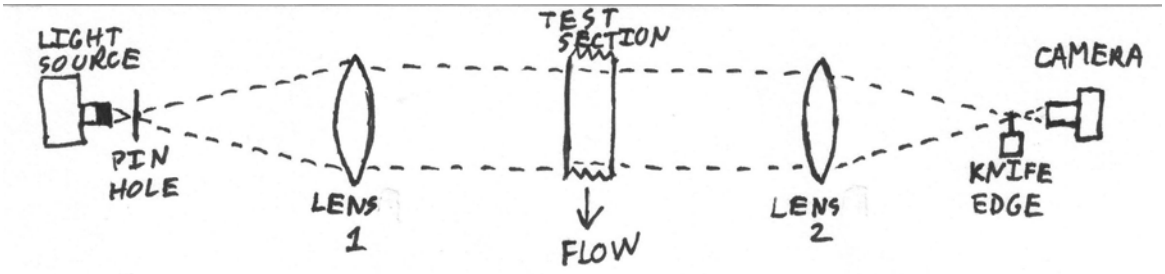

Figure 2-21. Traditional Schlieren implementation using lenses to generate a collimated beam.

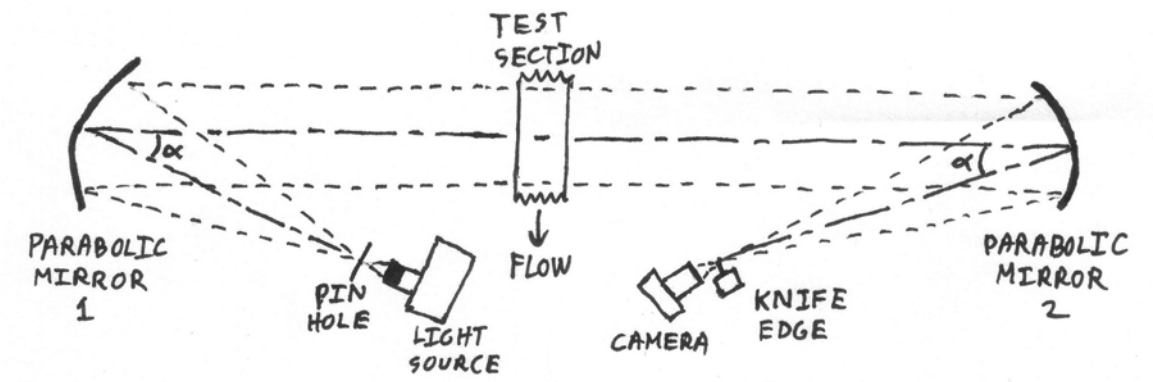

Figure 2-22. Schlieren implementation using parabolic mirrors to generate a collimated beam.

Parabolic mirrors of sizes, 9 5/8 inch diameter and 8 inch diameter, are used in the current schlieren setup. The first mirror is the 9 5/8 inch diameter mirror. The focal length of this mirror is long enough to allow the light source to sit on the laser sheet optics table and the mirror on the LDV optics table. With the point source at the focal point of the mirror, the mirror creates a collimated beam. This beam does not converge or diverge. Collimation was verified by measuring and matching the image diameter with the mirror diameter at 4 meters away from the mirror. To meet space limitations, the eight inch diameter mirror was used as the second mirror because it has a shorter focal length, 39 7/8 inches.

The 9 5/8 inch diameter mirror was initially tried as the second mirror, but the space limitations behind the test rig dictated that the mirror would have to turn the beam 90 degrees to allow enough distance for the beam to focus. This set up however, is less than optimal because the large turning of the beam will cause astigmatism and render the image useless. A flat mirror however, can be used to turn the beam without causing astigmatism. So, an industrial grade sixteen by sixteen inch flat, front surface mirror was purchased for this purpose and the optical system illustrated in Figure 2-23 was constructed. It was quickly discovered that the flat mirror added unexpected distortion to the image, indicating that it is not of high enough quality to be used for this purpose and was removed. A higher quality flat mirror could be purchased, but is cost prohibitive for this project. Therefore, this set up was forgone in favor of a more cost effective method. The second mirror in the set up was replaced with one of the 8 inch diameter mirrors,

which has a shorter focal length. This change permitted the camera and knife edge to fit between the second mirror and the test section, as previously shown in Figure 2-22.

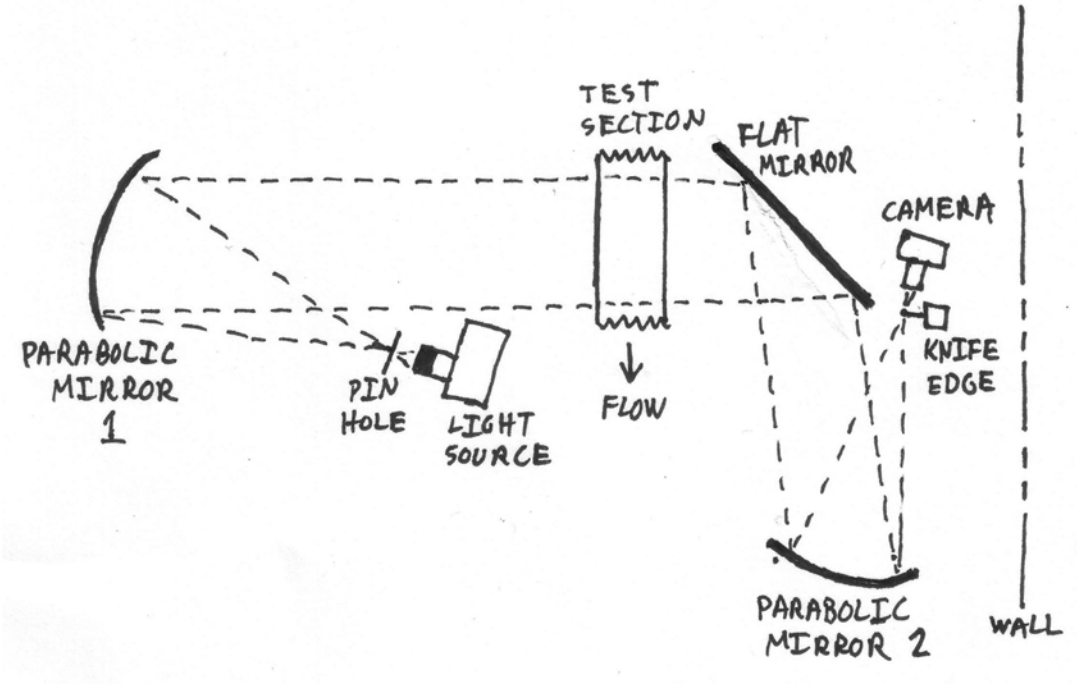

Figure 2-23. Schlieren implementation incorporating a flat mirror for beam turning to conserve space.

Schlieren flow visualization is often used to visualize flows where large density gradients exist, such as supersonic flow with shocks. In the current study, density gradients are achieved by mixing two gases of different density. Air is passed through the air inlets of each nozzle and helium is passed through the fuel inlets. At standard conditions, these gases provide a density ratio of 7.1:1, the air is 7.1 times denser then helium. Helium was also selected for the 'fuel' gas because it is inert, and therefore safe to handle in the lab.

For a successful schlieren implementation, a high intensity light source is required. In the current study, a 150 W xenon arc lamp is used as a source and a 200 W mercury arc lamp bulb was purchased as a spare. The power consumption of the xenon lamp is stable once set at the lamp power supply, but the mercury bulb is not. If the mercury lamp is installed, care must be taken to monitor the power consumption of the lamp. Once burning, the power consumption of the mercury arc will begin to increase on

its own. If the power is not carefully monitored, the lamp can go over power and explode. The lamp housing is designed to contain such an explosion, but damage to the components, such as expensive lenses, in the housing may occur. The manuals for the Oriel model 66058 lamp and model 68806 power supply can be found in the RFL equipment files, and their instructions should be precisely followed.

Optimally, the light source should act as a point source located at the focal point of the first mirror. This is achieved by using a 1280/215-1813 doublet lens assembly to focus the arc lamp into a pinhole. The only light reaching the mirror is the light from the pinhole at its focus, as all other light is blocked. A custom lens holder was constructed to mount the lens between the lamp and pinhole. Many available lenses and lens positions were evaluated to determine the optimal lens to use. The lens selection was complicated because the arc from the xenon lamp produces a rectangular image, which is difficult to focus down to a point. The optimal lens focuses a maximum amount of light into the pinhole and provides a beam divergence that will allow the mirror to capture a maximum amount of light from the pinhole. If the lens focuses light into the pinhole that diverges quickly after the pinhole, a large percentage of the light will not connect with the mirror and will be lost.

The optimal lens and pinhole configuration is shown in Figure 2-24. The pinhole used is approximately 1/16 inch in diameter. The assembly of the light source, lens, and pinhole is mounted on a platform with adjustable height legs to provide precision aiming. The set up of mirrors, pinhole and knife edge can easily be aligned by replacing the light source with a laser and mounting wire cross hairs on the mirrors. In this case, an available HeNe laser is used. Music is used to form a cross hair centered on each mirror. The laser beam should hit each cross hair in the center and hit the center of the knife edge. The optical system can also be aligned by placing screens behind the mirrors and noticing any light shining off of the mirror surfaces. Alignment should be performed in the dark because it is much easier to see the schlieren light beam.

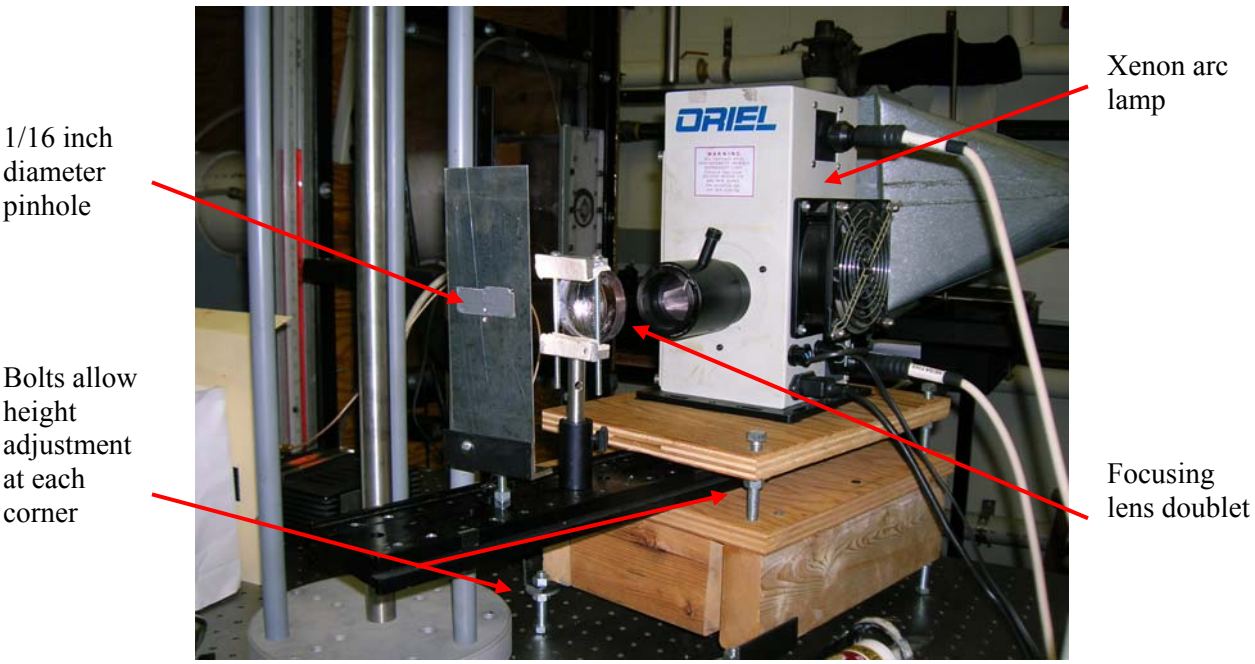

Figure 2-24. Schlieren light source assembly including xenon arc lamp, lens doublet, pinhole, and adjustable mounting hardware.

The knife edge is located on the opposite end of the optical system from the light source, and allows the image to be darkened providing clearer results. In Reference [3], Goldstein suggests that with an optimal knife edge implementation, where the knife edge is located at the focal point of mirror two, the image should be able to be uniformly darkened by further inserting the knife edge into the focal point. This uniform darkening was found to be difficult to achieve in the actual set up. At best, half of the image could be darkened uniformly.

Many knife edge types and configurations were explored. These include: flat, angled, and round knife edges in different locations and orientations. It was concluded that bringing a flat knife edge in from the bottom of the image yielded the most uniform darkening. Obtaining an optimal knife edge setting is critical for visualizing the well mixed flow at design conditions. With this in mind and an optimal knife edge type and orientation selected, the knife edge position remained to be optimized. The optimization process is facilitated by the construction of an apparatus that allows fine adjustment of the knife edge in two axes. The apparatus shown in Figure 2-25 allows fine translation

along the axis of the light beam and along the vertical axis, as indicated by the green arrows.

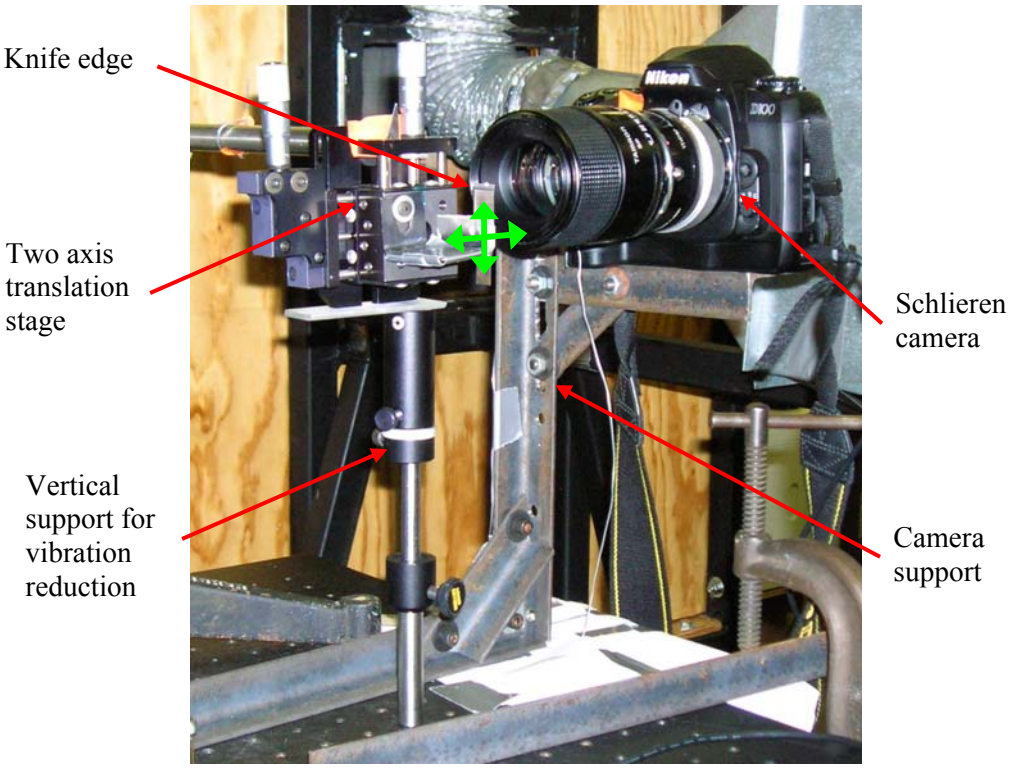

Figure 2-25. Knife edge and translation stages for fine positioning. Image captured by Forero [6].

As mentioned previously, placing the knife edge in the focal plane of the second mirror allows for uniform darkening of the image. The ability to translate along the axis of the light beam permits accurate positioning of the knife edge in the focal plane. Results of optimization revealed that the most uniform image darkening is achieved with the knife edge positioned 0.1 inches beyond the focal plane. The overall sensitivity is adjusted by fine tuning the vertical position of the knife edge as it enters the focal point. Goldstein, [3] recommends that if a_0 and b_0 are the dimensions of the focal point, the shorter of the two should be placed perpendicular to the knife edge, as illustrated in Figure 2-26. Maximum sensitivity is achieved when the knife edge is placed at $a_k=a_0/2$.

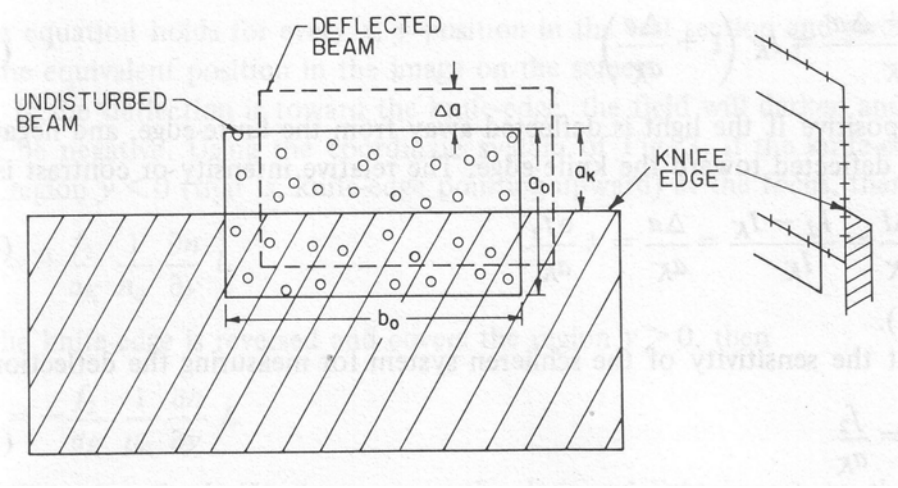

Figure 2-26. Image illustrating knife edge placement at the focal point of the second mirror [3].

A Nikon D-100 camera, as seen in Figure 2-25, is used to capture the schlieren images. Rigorous study of several camera positions indicated that the camera should be located after the knife edge with the light directly entering the camera. Six lens combinations were evaluated for the camera along with several camera settings to arrive at an optimal image. The camera is mounted on a custom built mounting bracket which allows its position and angle to be optimized and set. The camera was set to take the largest images at the finest resolution, to have the widest field of view, and best quality.

Six lens combinations were studied to find the lens which provided the sharpest and brightest image. The following lenses were studied; Nikon 50mm, Tokina 28mm, and the Tamron SP 90mm, each with and without a Vivitar 3x Automatic Tele Converter (ATC). The lens study showed that the Tamron SP with ATC provided the optimal image for the current schlieren implementation. The lens f-stop was set at 2.5, fully open for this lens.

This study is predominantly aimed at capturing and analyzing one image from each nozzle at on-design fuel and air mass flow rates; however, it is challenging to properly interpret the schlieren images taken at this condition because there are few density gradients to observe. To overcome this challenge, a series of images is taken at increasing air flow rates starting with an air flow which provides large, clear density gradients and working up to the on-design conditions. This is accomplished by holding the fuel flow constant at 100% of design and ramping the air flow up to 100% design in

15 to 20% steps. A series of ten images are recorded at each flow rate, and the clearest image is saved for processing. These processed images are presented and discussed in Chapters 3 and 4.

Two similar MATLAB m-files, both in Appendix G, were written to post process the schlieren images. 'ProcessJ.m' is used to process the images of Nozzle J and 'processD.m' is used to process the images of nozzle D. These codes are identical with the exception of lines 7, 9, 16, 33, and 36, which are specific to the particular nozzle. Each code contains five separate commented processes. First, the code reads a schlieren image into MATLAB, then it crops the image to show only the area of interest. After the image has been cropped, its intensities are rescaled using the following process: the code finds the maximum intensity in the image and sets this to the highest pixel value of 255, then it finds the lowest intensity and sets this to the lowest pixel value of 0 and rescales all of the other pixels to use the full range, 0-255. This process maximizes the image contrast and therefore, the clarity of density gradients. Finally, the processed image is saved as a jpeg file and can be displayed automatically if the 'display' input is set to 1. All of these processes are contained within a 'for loop' controlled by the 'number' input, which sets the number of images to be batch processed.

2.2.3 LDV Velocity Measurement System

As mentioned in Section 1.2.3 a two axis, dual beam, backscatter LDV is implemented in this study. The RFL LDV system (optics, electronics, and software) was originally designed and constructed by Dr. Haber. To increase mobility, the LDV optics have since been relocated to a new optical table. Before the current study, the original LDV ceased to operate correctly and after troubleshooting the optical system, the custom built processing electronics were suspected to be the problem. These electronics proved difficult to troubleshoot and diagnose, so a new electronics package was developed. The new electronics also required the development of new software for data collection and processing.

The new electronics package is composed of new PMT amplifiers and a pair of TSI, Inc. Counter Timer processors. These PMT amplifiers have increased gain and

reduced noise over the original design. The counter timers replace the processing electronics and are simpler to operate and troubleshoot. The LDV electronics package and processing software are discussed in this section, while the procedures used to conduct an LDV measurement are discussed in great detail in Appendix C.

The LDV electronics begin with the PMTs. Scattered light returned from the probe volume is split into green and blue components by a dichroic mirror, each component is then band pass filtered before entering the PMT housings. The PMT housing and circuitry are identical for the green and blue components, so only one is discussed here. An open PMT housing is shown in Figure 2-27. Inside the PMT, photons strike a photocathode, which releases electrons. These electrons are accelerated through a high voltage field (typically 1 to 3 kV) and impact a series of dynodes, which each release more than one electron for each striking electron. This operation amplifies the electron output and a current is generated. Following manufacturer recommendations, the dynodes are connected together, and the output is connected to the high impedance amplifier circuit shown.

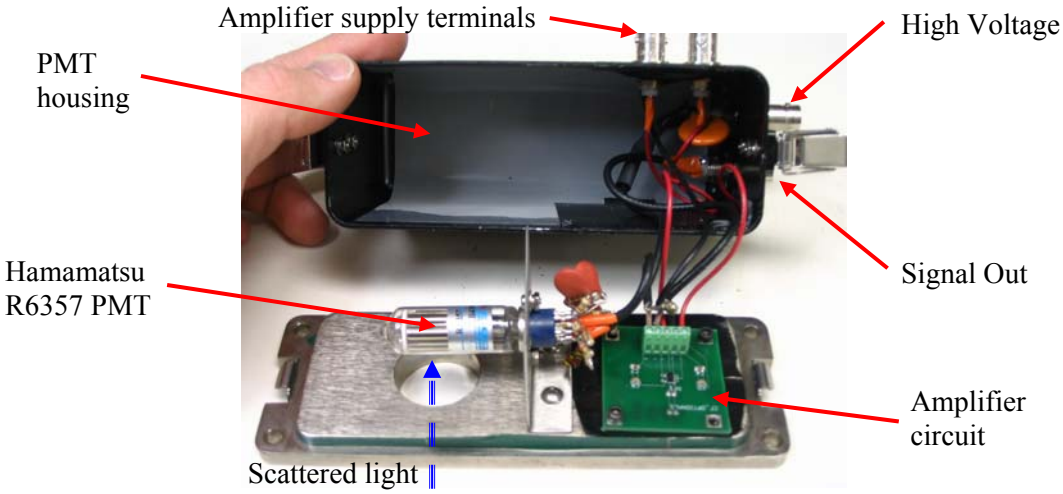

Figure 2-27. Image showing an opened PMT housing including PMT and custom designed amplifier circuit.

Figure 2-28 shows the amplifier circuit diagram as installed. The 100 kΩ feedback resistor sets the gain to 10^5 and the amplifier is supplied by ±12 Volts. The Analog Devices 8065 amplifier was selected for its high bandwidth and low noise. The

gain is set high enough that applying a PMT supply voltage of greater then 400 volts will saturate the amplifier output.

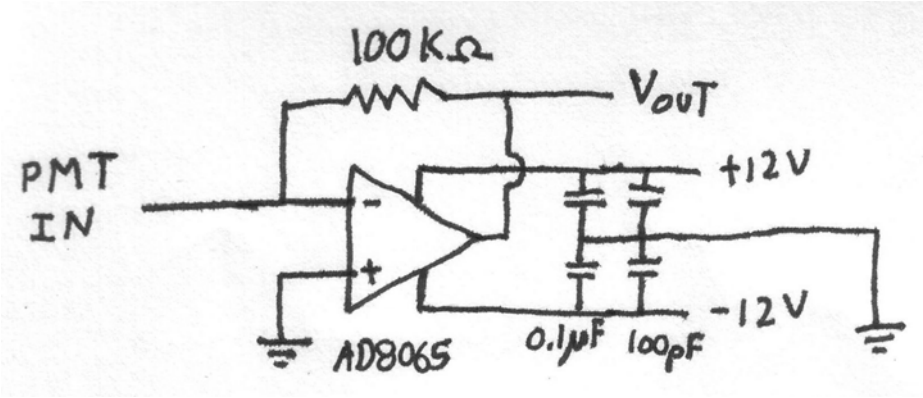

Figure 2-28. Schematic diagram of the PMT amplifier circuit with 10^5 gain.

The PMT signal for each color is delivered to a separate counter timer and is connected to the input conditioner module on the counter timer. The input conditioner module has both a high and low limit filter. The low limit filter passes frequencies above its setting and attenuates those below to remove the pedestal part of the LDV signal. The high limit filter passes frequencies below its setting to remove any noise that could be interpreted as valid data. An oscilloscope can be connected to the 'Filtered Out' terminal to observe the clean output of the conditioner.

After the input has been conditioned, the counter timer counts the number of cycles within a Doppler burst. If the number of cycles counted is equal to or greater than the number set by the 'Cycles/Burst' control, the burst is passed to the timer module, and all other bursts are thrown out. The timer module determines the frequency of the Doppler signal and validates the output internally by checking if any of the following conditions exist:

1) amplifier saturation detected during measurement
2) amplitude limit is exceeded during measurement
3) the time measured exceeds 2^{24} counts

Once a frequency is validated, it is latched to the 'Monitor' output and a 0.5 μs Transistor to Transistor Logic (TTL) pulse is issued to the 'Data Ready' output. On the 'Monitor'

output, frequency is provided as a DC voltage from 0 to 10 volts and Equation 2-1, as given in the counter timer manual, is used to convert the voltage back into a frequency.

$$F = \frac{(N)(10^{10})}{(V_M)(2^{EXP+9})} \tag{2-1}$$

In this equation, N is the cycles/burst set on the conditioner module, V_M is the voltage at the monitor output, and EXP is the value of the exponent set on the timer module using the following formula:

$$EXP = (S_1)(1) + (S_2)(2) + (S_4)(4) + (S_8)(8) \tag{2-2}$$

where S_n=1 if the switch next to the label n is depressed, S_n=0 otherwise [4].

To successfully read a frequency from each counter timer, both the 'Monitor' and 'Data Ready' signals must be sampled, four signals in all. After much effort using a standard Data Acquisition (DAQ) board with 8 channels, it was determined that a high speed DAQ was needed to accurately capture the pulses in the 'Data Ready' signal. The high speed DAQ available in the RFL has only two input channels, and therefore the green and blue signals can not be measured coincidently. This is acceptable because this study is only interested in independent measurement of the mean velocity of each component. Coincident component measurement is required if the interest is in the velocity spectra (FFT) or the computation of velocity statistics. Another challenge presented by the high speed DAQ board is that its input is limited to a -5 to +5 voltage range. To solve this problem, the counter timer output must be shifted down 5 Volts before acquisition, and then raised back up in software.

In an effort to overcome the two challenges discussed with the high speed DAQ board, a low frequency multiplexer with -5 Volt DC offset was created. This multiplexer, shown in Figure 2-29, includes two components, a low current signal relay (OMRON G5A-234P) and a dual op-amp circuit to provide the offset. The electrical schematic for these two circuits is shown in Figure 2-30. A 5 volt digital signal from the National Instruments (NI) DAQ board in the LDV computer can control the relay, which has four inputs and two outputs. When "off," the blue 'monitor' and 'data ready' signals are passed to the output and when "on," the green signals are passed to the output. The 'data ready' signal is connected directly from the relay to the output terminal while the 'monitor' signal is first processed by the dual op-amp circuit before going to the output

terminal. The National Semiconductor LMC6482IN contains two op-amps which have been connected in series. The first op-amp sums the -5 volt signal with the 'monitor' signal from the relay and inverts it. The second op-amp again inverts the signal to undo the inversion of the first op-amp. All 5 resistors used in the circuit are 1MΩ and both amplifiers have unity gain.

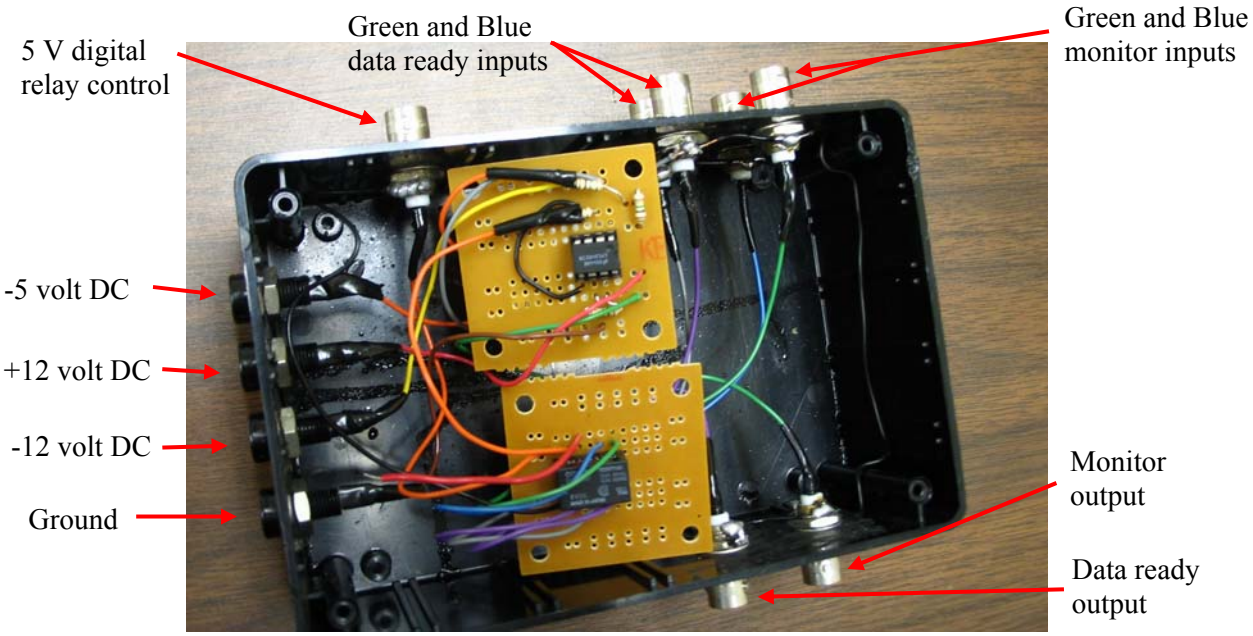

Figure 2-29. Photograph of the low frequency multiplexer with -5 volt DC offset.

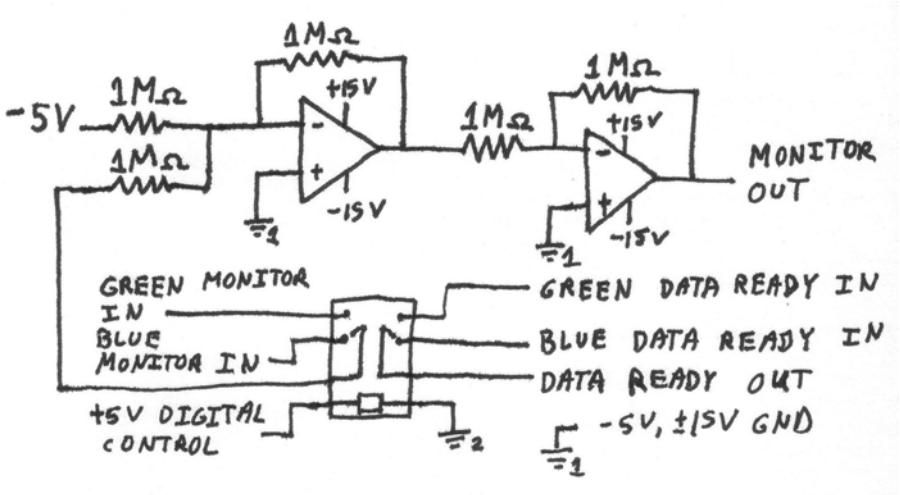

Figure 2-30. Electrical schematic of the multiplexer with -5 volt DC offset. Both op-amps are contained within a dual DIP package. Also note that the 'high' current relay control ground is separate from all other grounds to reduce noise.

The ‘monitor’ and ‘data ready’ outputs from the multiplexer are captured by the high speed DAQ card and pulled into LabVIEW for processing. Several LabVIEW VI’s were written to capture and process the LDV data. These include: ‘FastLDVCheck.vi,’ ‘LDVFastCapture.vi,’ ‘Valid.vi,’ and ‘VelocityCalc.vi.’ ‘FastLDVCheck’ is the highest level VI which contains a sequence that calls ‘LDVFastCapture,’ to capture the ‘monitor’ and ‘data ready’ signals, and then calls ‘Valid’ which locates all valid triggers in the ‘data ready’ signal, and then runs ‘VelocityCalc’ to convert the voltages into velocities. Each VI is commented for understanding of its internal operation.

‘FastLDVCapture’ will take a series of samples; compute the mean velocity for each sample, and compute the mean velocity for all of the samples. The number of samples recorded is controlled by the ‘Number of Iterations’ input on the front panel. A histogram of the mean velocity from each sample is also produced so the user can evaluate confidence in the overall mean.

‘LDVFastCapture’ captures the ‘monitor’ and ‘data ready’ signals until the DAQ buffer is nearly full. It then reads from the buffer, adds 5 Volts back to the monitor signal, and saves both signals in a file specified by the user. Much of this VI is adapted from a GaGe oscilloscope VI. In the reading of one buffer, many triggers can exist in the ‘data ready’ signal. ‘Valid’ is run next and is responsible for determining which of the triggers captured are valid and which should be discarded. The logic used to validate the triggers is explained in the comments of ‘Valid.’ Once the valid triggers from the sample are identified, the ‘monitor’ signal array is sampled for a set time ‘w’ starting a time‘t’ after each trigger. The data sampled after each trigger are averaged together to determine an average voltage for each trigger, and then these averages are averaged together to find a single average voltage for the sample. This voltage is finally used by ‘VelocityCalc’ to compute the mean velocity for the sample in [m/s].

The ‘monitor’ signal is sampled for the limited time ‘w’ after each trigger to ensure that a new trigger does not occur during sampling. Sampling is initiated a time‘t’ after the trigger to ensure that the ‘monitor’ signal is not sampled during its rise or decay time to a new value. Figure 2-31 illustrates the trigger and sampling process described for the ‘monitor’ and ‘data ready’ signals.

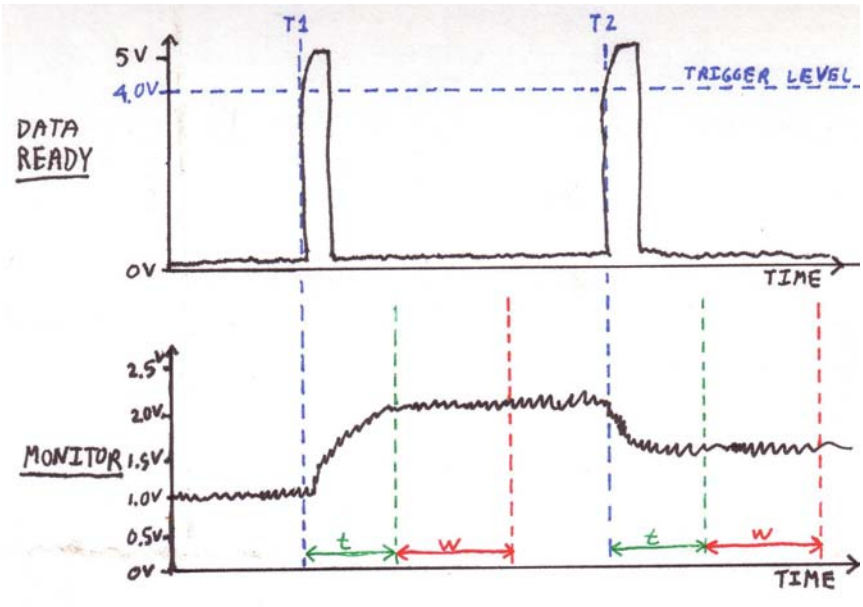

Figure 2-31. Illustration of trigger and 'monitor' array sampling process in 'Valid.vi.'

The previous discussion illustrates the current capability of the LDV system to measure mean velocity in a test configuration. For testing purposes, the LDV probe has been mounted on the LDV optics table, measuring the velocity of an air jet seeded with water droplets. The seeded flow is generated by a TSI model 9306 six-jet atomizer located below the LDV optics table and supplied with air from the RFL compressor. The seeded flow is delivered to the probe volume by a ½ inch o.d. tube. A Matheson 605 rotameter, calibrated against a Singer dry gas meter, is used to measure the flow rate of the air before it enters the atomizer. Because the outlet flow from the atomizer is turbulent and therefore does not have a defined velocity profile, a quick (mass flow)=ρVA calculation is used to compute the velocity at the tube outlet. This set up provides a consistent seed density and mean velocity standard to compare with LDV results. The angle of the atomizer tube is used to compute the velocity components that should be measured by the two components of the LDV. Figure 2-32 shows the LDV probe and atomizer set up.

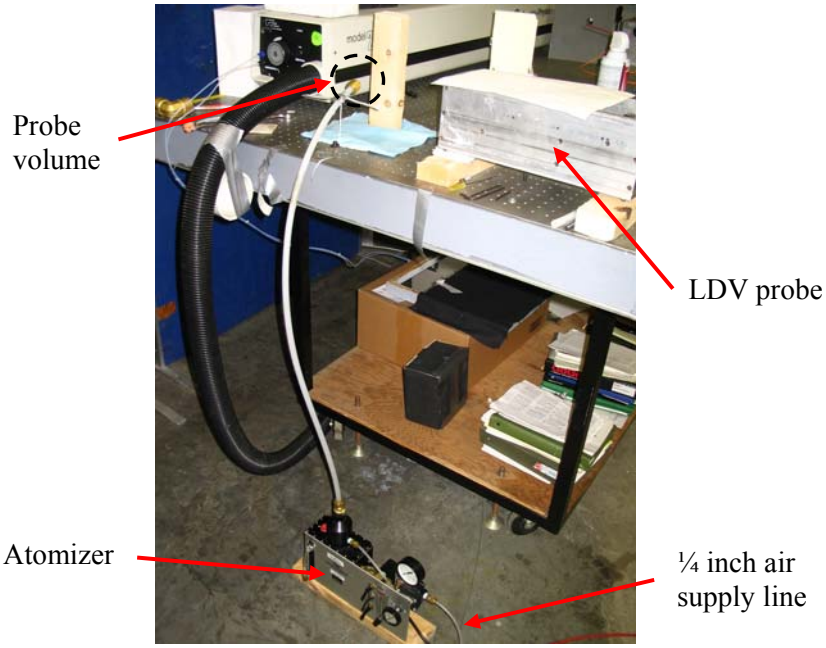

Figure 2-32. Photograph of TSI atomizer and LDV probe set up for LDV testing.

The results obtained from the LDV testing with the atomizer are presented in Section 3.3. These results indicate the current performance of the LDV. Future plans for and the potential of the LDV are also discussed.